AF Project 700100
Interim Technical Report

the ohio state university
research foundation
1314 kinnear road
columbus, ohio
43212

(2)

IGNITION, COMBUSTION, DETONATION, AND QUENCHING OF REACTIVE MIXTURES

R. Edse and O. Dhiman
Department of Aeronautical and Astronautical Engineering

December 1977

AIR FORCE OFFICE OF SCIENTIFIC RESEARCH
Bolling Air Force Base
Washington, D. C. 20332

Qualified requestors may obtain additional copies from the Defense Documentation Center, all others should apply to the National Technical Information Service.

UNCLASSIFIED

SECURITY CLASSIFICATION OF THIS PAGE (When Data Entered)

REPORT DOCUMENTATION PAGE	READ INSTRUCTIONS BEFORE COMPLETING FORM
1. REPORT NUMBER: AFOSR-TR-78-0956	2. GOVT ACCESSION NO. / 3. RECIPIENT'S CATALOG NUMBER
4. TITLE (and Subtitle): IGNITION, COMBUSTION, DETONATION, AND QUENCHING OF REACTIVE MIXTURES	5. TYPE OF REPORT & PERIOD COVERED: Interim Rept. 1 Apr [illegible]76 - 31 Mar [illegible]77
	6. PERFORMING ORG. REPORT NUMBER: ORF-76100/783641
7. AUTHOR(s): Rudolph Edse, Om Dhiman	A035-486
	8. CONTRACT OR GRANT NUMBER(s): AFOSR-73-2511
9. PERFORMING ORGANIZATION NAME AND ADDRESS: The Ohio State University Research Foundation - 1314 Kinnear Road, Columbus, Ohio 43212	10. PROGRAM ELEMENT, PROJECT, TASK AREA & WORK UNIT NUMBERS: 2308A2, 61102F
11. CONTROLLING OFFICE NAME AND ADDRESS: Air Force Office of Scientific Research (NA), Building 410, Bolling Air Force Base, Washington, D. C. 20332	12. REPORT DATE: Dec [illegible]77
	13. NUMBER OF PAGES: 79
14. MONITORING AGENCY NAME & ADDRESS (if different from Controlling Office): 87p.	15. SECURITY CLASS. (of this report): Unclassified
	15a. DECLASSIFICATION/DOWNGRADING SCHEDULE

16. DISTRIBUTION STATEMENT (of this Report)

Approved for public release; distribution unlimited.

17. DISTRIBUTION STATEMENT (of the abstract entered in Block 20, if different from Report)

18. SUPPLEMENTARY NOTES

19. KEY WORDS (Continue on reverse side if necessary and identify by block number)

Deflagration; Detonation; Transition; Induction Distance; Flame Acceleration; Wave Speed; Hydrogen; Bromine; Turbulence; Real Gas Effect; Quenching; Detonability; Reaction Rate; Reaction Zone; Rotational Temperature; Nonequilibrium; Flame Speed; Flame Arrestor; Shock Wave; Shock Tube; C.J. Detonation; Overdriven; Driver Gas; Ignition; Catalysis; Methane; Acetylene

20. ABSTRACT (Continue on reverse side if necessary and identify by block number)

A one mole hydrogen - one mole bromine mixture has been detonated by shock ignition. To distinguish the shock wave driven into the hydrogen-bromine mixture from a detonation wave which may have formed, the measured wave speeds and pressures were compared with theoretically calculated values. The experimental data were found to be nearly equal to those of the C.J. detonation wave. Calculations of the reaction zone thickness of the wave show that the straight chain reaction mechanism for the hydrogen bromide formation can sustain stable detonation waves. Several series of experiments to quench flames of various gaseous fuel-air

DD FORM 1 JAN 73 1473 EDITION OF 1 NOV 65 IS OBSOLETE

UNCLASSIFIED

SECURITY CLASSIFICATION OF THIS PAGE (When Data Entered)

267 360

Block 20 (Con't)

mixtures were carried out with three different flame arrestors. The most useful device is a rectangular burner with a large length-to-width ratio. The bunsen type flames were quenched by squeezing them between two movable blocks, which were made from different materials and coated with catalysts and inhibitors. The steady-state condition of various phases of the quenching process, which this device can produce, has made spectroscopic studies possible. These observations revealed that nonequilibrium states are formed during the quenching process. The effects of flame speed, Reynolds number, temperature, catalysis, and roughness of the flame arrestor have been studied. Quenching distances have been measured for methane-air, methane-oxygen, acetylene-air, and hydrogen-air mixtures, with blocks of copper and mica. Third-gas additives to these mixtures have been used to determine the influence of the chemical composition of the combustible gas mixture on the effectiveness of the flame arrestor. Quenching distances were found to be independent of the shape of the burner, the linear gas speed, and the Reynolds number of the unburned gas. However, they depend on flame speed, flame temperature, and the nature and material of the quenching surface. Preliminary experiments were carried out to determine the effect of initial gas density on the induction distance of hydrogen-oxygen-third-gas mixtures. A new apparatus for studying the effect of external turbulence on the induction distance is under construction.

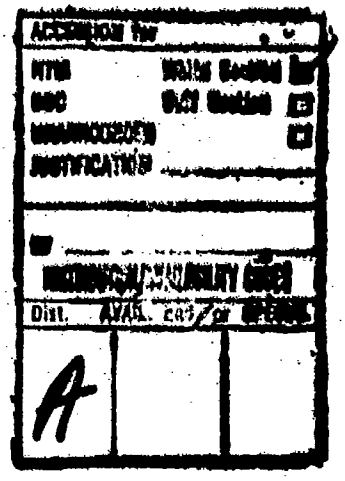

TABLE OF CONTENTS

LIST OF TABLES

LIST OF TABLES (Continued)

LIST OF FIGURES

LIST OF FIGURES (Continued)

LIST OF FIGURES (Continued)

LIST OF SYMBOLS

$a^{(j)}$	Coefficient of equilibrium constant for reaction j
c_i	Concentration of species i in mixture (mol/ℓ)
$\left(\frac{C_p}{\mathcal{R}}\right)_i^T$	Dimensionless specific heat at constant pressure of species i at temperature T
$\left(\frac{H_f}{\mathcal{R}T}\right)_i^T$	Reduced formation enthalpy of species i at temperature T; elements at T = 0 K
$\left(\frac{H-E_0}{\mathcal{R}T}\right)_i^T$	Reduced sensible enthalpy of species i at temperature T
$K_p^{(j)}$	Equilibrium constant of reaction j in terms of partial pressures $p^{\Delta\nu^{(j)}}$
L_r	Length of reaction zone of detonation wave in mm
$k^{(j)}$	Reaction rate constant of reaction j
$\mathcal{M}$	Molecular mass (kg/kmol)
p	Static pressure in atm
p_i	Partial pressure of species i in gas mixture
$\mathcal{R}$	Universal gas constant; 8314.33 (J/kmol K)
$R = \mathcal{R}/\mathcal{M}$	Specific gas constant (J/kg K)
$\left(\frac{S^{p=1}}{\mathcal{R}}\right)_i^T$	Dimensionless standard entropy of species i at temperature T
T	Absolute temperature K
u	Gas speed in (m/s)
$v = 1/\rho$	Specific volume in (m^3/kg)
w	Wave speed in (m/s)
w_a	Speed of sound in (m/s)

$\gamma = c_p/c_v$	Ratio of specific heats
$\eta_i = p_i/p$	Mole fraction of species i in mixture
$\nu_i^{(j)}$	Stoichiometric mole number of species i in reaction j
M.E.R.	Maximum Energy Release

SUBSCRIPTS

1	Denotes state of initial unreacted gas mixture
2	Refers to state of unreacted gas mixture at tail of normal shock
r	Refers to state of reacted gas mixture in complete equilibrium at tail of detonation wave
3	Refers to state of driver gas at tail of expansion wave
4	Denotes state of initial driver gas
i	Denotes any of the species H_2, Br_2, H, Br, HBr

SUPERSCRIPTS

j	Denotes a particular reaction; j = 1, 2, or 3
C.J.	Refers to Chapman-Jouguet detonation
s. eq.	Denotes shifting equilibrium
f. eq.	Denotes frozen equilibrium
calc.	Refers to calculated value

IGNITION, COMBUSTION, DETONATION, AND QUENCHING OF REACTIVE GAS MIXTURES

I. DETONABILITY OF A ONE MOLE HYDROGEN-ONE MOLE BROMINE MIXTURE

A. INTRODUCTION

It is a generally accepted fact that in ordinary flames of hydrogen-bromine mixtures the reaction mechanism is that of a simple straight chain without branching. This mechanism has been established for many years.[1,2] Because of the rather slow overall reaction rate provided by an unbranched chain mechanism, it may be expected that a stable detonation wave in hydrogen-bromine mixtures does not exist. All mixtures which are known to detonate involve a chain-branching mechanism. The study of the flame propagation rate and shock ignition of hydrogen-bromine mixtures was undertaken to obtain some insight into the detonability of low-energy mixtures and to gather more information on the transition from deflagration to detonation.

B. THEORETICAL ANALYSIS

1. Calculation of the State of the Gas Mixture Behind Normal Shock and Detonation Waves Passing Through Hydrogen-Bromine Mixtures

The detonation speeds and the pressures behind the waves were calculated for a one mole hydrogen-one mole bromine mixture at an initial temperature, T_1, of 313 K and an initial pressure, p_1, of one atmosphere. The calculations are started with an assumed value of the temperature at the tail of the detonation wave, T_r, for which, the associated pressure, p_r, was obtained from the Hugoniot equation:

$$p_r^{calc} = p_1\Big[a(b - 0.5) - (c - 0.5) + \{[a(b - 0.5) - (c - 0.5)]^2 + a\}^{0.5}\Big], \qquad (1)$$

where $$a = \frac{T_r}{T_1} \cdot \frac{m_1}{\sum \eta_{i,r} m_i}, \qquad b = \sum \eta_{i,r} \left(\frac{H_f}{RT}\right)_i^{T_r}, \text{ and}$$

$$c = \sum \eta_{i,1} \left(\frac{H_f}{RT}\right)_i^{T_1}.$$

These calculations involve an iterative procedure because the mole fractions, $\eta_{i,r}$, on the right hand side of this equation depend on p_r which, therefore, like the temperature has to be estimated so that the mole fractions of the detonated mixture can be calculated. The iterations were

continued until

$$100 \cdot \left| \frac{p_r^{calc} - p_r^{est}}{p_r^{calc}} \right| < \epsilon \simeq 0.1\% \ . \qquad (2)$$

Then with several compatible pairs of T_r and p_r values, the wave speeds were calculated according to the expression

$$w_1 = \left[\frac{\left(\frac{p_r}{p_1} - 1 \right) R_1 T_1}{1 - \frac{T_r}{T_1} \cdot \frac{m_1}{\sum \eta_{i,r} m_i} \cdot \frac{p_1}{p_r}} \right]^{0.5} , \qquad (3)$$

which is derived from the continuity and momentum equation. For temperatures ranging from 1506 to 3000 K the results of these calculations are compiled in Table I. The wave speed of the C.J. detonation, $w_1^{C.J.}$, can be obtained by two methods; i.e., (1) by determining the minimum of the calculated wave speeds, w_1, as shown in Fig. 1, which represents the relationship between w_1 and T_r; and (2) from the condition that $M_{w_r}^{C.J.} = \frac{w_r^{C.J.}}{w_{a,r}^{s.eq.}} = 1$, where $w_r^{C.J.} = w_1^{C.J.} \cdot \frac{v_r^{C.J.}}{v_1}$ is the wave speed relative to the detonated gas and $w_{a,r}^{s.eq.}$ is the equilibrium speed of sound in this gas:

$$w_{a,r}^{s.eq.} = \left[\frac{\gamma_r^{s.eq.} \cdot \Re T_r}{\sum \eta_{i,r} m_i} \right]^{0.5} , \qquad (4)$$

where

$$\gamma_r^{s.eq.} = \frac{\sum \eta_i \left(\frac{C_p}{\Re} \right)_i + \left[\frac{\Delta H^{(\ell)}}{\Re T} \right] \left[a_{\ell j} \right]^{-1} \left\{ \frac{\Delta H^{(j)}}{\Re T} \right\}}{\sum \eta_i \left(\frac{C_p}{\Re} \right)_i - 1 + \left[\frac{\Delta H^{(\ell)}}{\Re T} - \Delta \nu^{(j)} \right] \left[b_{\ell j} \right]^{-1} \left\{ \frac{\Delta H^{(j)}}{\Re T} - \Delta \nu^{(j)} \right\}}$$

$$\cdot \frac{1 + \left[\frac{\Delta H^{(\ell)}}{\Re T} \right] \left[\Delta \nu^{(\ell)} \right] \left[b_{\ell j} \right]^{-1} \left\{ \Delta \nu^{(j)} \right\}}{1 + \left[\frac{\Delta H^{(\ell)}}{\Re T} \right] \left[a_{\ell j} \right]^{-1} \left\{ \Delta \nu^{(j)} \right\}} , \qquad (5)$$

where

Table I. Detonation parameters calculated for a 1 mole hydrogen - 1 mole bromine mixture (T_1 = 313 K, p_1 = 1 atm)

w_1 (m/s)	M_{w_1}	w_2 (m/s)	p_2 (atm)	T_2 (K)	w_r (m/s)	f. eq. M_{w_r}	s. eq. M_{w_r}	p_r (atm)	T_r (K)
0	0	Ideal Constant Pressure Combustion						1.00	1506
∞	∞	Ideal Constant Volume Combustion						6.48	1988
1905	9.165				1802.6	3.417	—	6.99	2000
951.4	4.577	Supersonic Combustion Without Shock Wave (Weak Detonation)			626.82	1.156	—	10.60	2100
931.71	4.485				545.89	0.995	—	12.18	2140
931.14					538.19			12.38	2145
930.90	4.4787				531.18	0.966	1.0097	12.59	2150
930.81	4.4786	170.6	23.006	1319.6	526.55	0.957	1.0000	12.70	2153*
931.04	4.4794	170.6	23.016	1320	516.98	0.938	0.9801	12.99	2160
939.6	4.521	171.3	23.44	1338	472.35	0.848	—	14.65	2200
989.3	4.759	175.9	25.96	1445	403.89	0.706	—	19.01	2300
1197.7	5.762	195.4	38.34	1958	321.06	0.520	—	33.65	2600
1480.2	7.121	222.8	58.88	2774	288.33	0.423	—	55.85	3000

*C.J. detonation

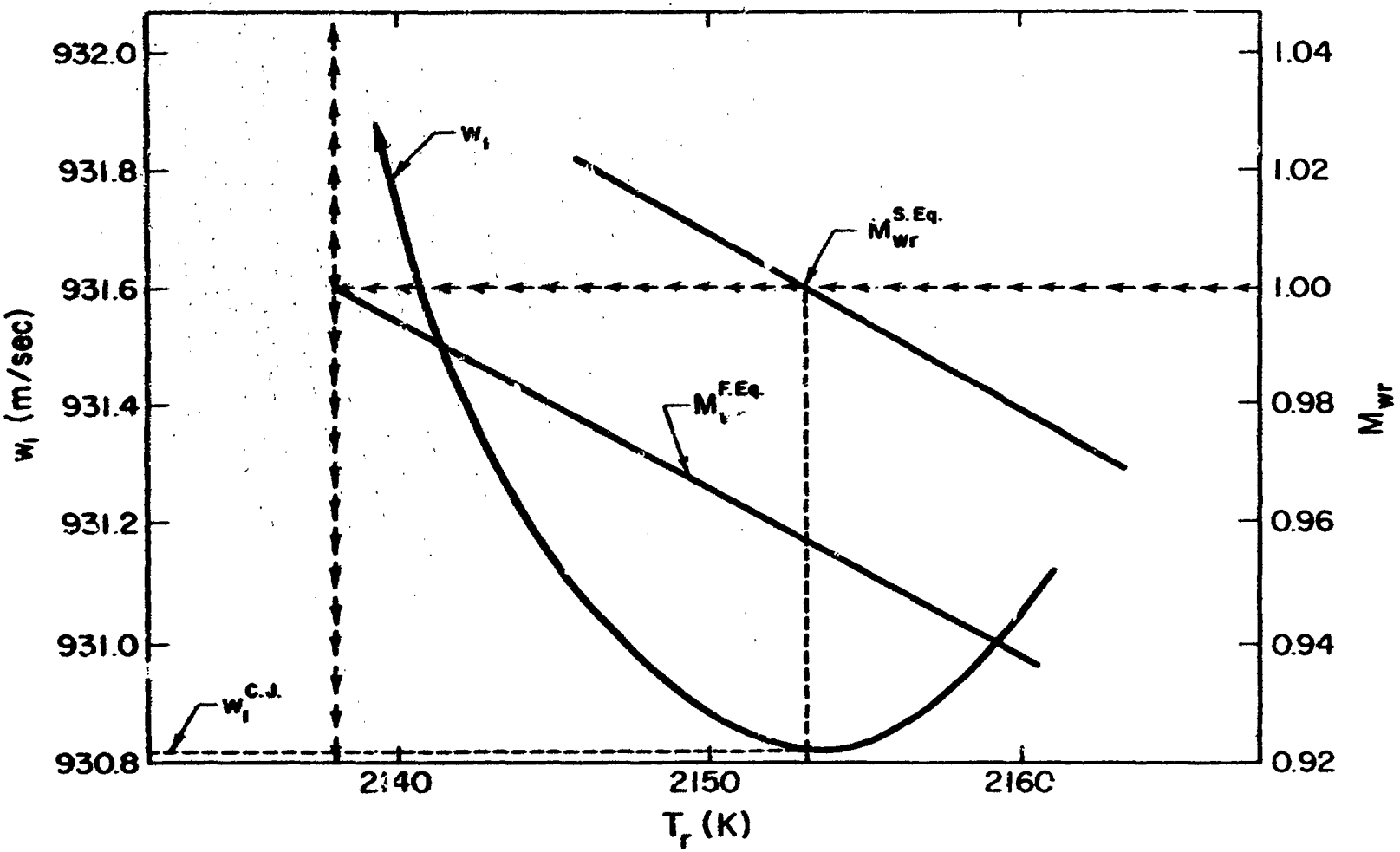

Fig. 1 - Wave speed as a function detonated gas temperature for a $1H_2 + 1Br_2$ mixture initially at 313 K and 1 atm

$$a_{\ell,j} = b_{\ell,j} - \Delta\nu^{(\ell)} \cdot \Delta\nu^{(j)} ,$$

$$b_{\ell,j} = \sum_i \frac{\nu_i^{(\ell)} \cdot \nu_i^{(j)}}{\eta_i} , \text{ and}$$

$$\frac{\Delta H^{(\ell)}}{\mathcal{R}T} = \sum_i \nu_i^{(\ell)} \left(\frac{H_f}{\mathcal{R}T}\right)_i^T .$$

For the three reactions (j or ℓ = 1, 2, and 3) governing the chemical equilibrium of hydrogen-bromine mixtures the stoichiometric mole numbers $\nu_i^{(\ell)}$ or $\nu_i^{(j)}$ and the expressions for the enthalpy changes $\Delta H^{(\ell)}$ or $\Delta H^{(j)}$ are listed in Tables II and III. The dimensionless reduced formation enthalpies were calculated by means of the following defining equation:

$$\left(\frac{H_f}{\mathcal{R}T}\right)_i^T = \left(\frac{H}{\mathcal{R}T}\right)_i^T - \sum_{el} \nu_{el}^{(i)} H_{el}^{T=0K} \cdot \frac{1}{\mathcal{R}T} ;$$

$$\left(\frac{H_f}{\mathcal{R}T}\right)_{H_2}^T = \left(\frac{H-E_o}{\mathcal{R}T}\right)_{H_2}^T + \frac{1}{T}\left(\frac{H_f}{\mathcal{R}}\right)_{H_2}^{T=0K} , \text{ where } \left(\frac{H_f}{\mathcal{R}}\right)_{H_2}^{T=0K} = 0 ; \quad (6)$$

$$\left(\frac{H_f}{\mathcal{R}T}\right)_{H}^T = \left(\frac{H-E_o}{\mathcal{R}T}\right)_{H}^T + \frac{1}{T}\left(\frac{H_f}{\mathcal{R}}\right)_{H}^{T=0K} , \text{ where } \left(\frac{H_f}{\mathcal{R}}\right)_{H}^{T=0K} = 25982 \text{ K} ; \quad (7)$$

$$\left(\frac{H_f}{\mathcal{R}T}\right)_{Br_2}^T = \left(\frac{H-E_o}{\mathcal{R}T}\right)_{Br_2}^T + \frac{1}{T}\left(\frac{H_f}{\mathcal{R}}\right)_{Br_2}^{T=0K} , \text{ where } \left(\frac{H_f}{\mathcal{R}}\right)_{Br_2}^{T=0K} = 0 ; \quad (8)$$

$$\left(\frac{H_f}{\mathcal{R}T}\right)_{Br}^T = \left(\frac{H-E_o}{\mathcal{R}T}\right)_{Br}^T + \frac{1}{T}\left(\frac{H_f}{\mathcal{R}}\right)_{Br}^{T=0K} , \text{ where } \left(\frac{H_f}{\mathcal{R}}\right)_{Br}^{T=0K} = 11437.66 \text{ K} ; \text{ and} \quad (9)$$

$$\left(\frac{H_f}{\mathcal{R}T}\right)_{HBr}^T = \left(\frac{H-E_o}{\mathcal{R}T}\right)_{HBr}^T + \frac{1}{T}\left(\frac{H_f}{\mathcal{R}}\right)_{HBr}^{T=0K} , \text{ where } \left(\frac{H_f}{\mathcal{R}}\right)_{HBr}^{T=0K} = -6155.208 \text{ K} . \quad (10)$$

The dimensionless sensible enthalpies are listed in Table IV and dimensionless specific heats, $\left(\frac{C_p}{\mathcal{R}}\right)_i^T$ are tabulated in Table V. The equilibrium constants $K_p^{(j)}$ can be expressed by the general equation

$$K_p^{(j)} = a^{(j)}{}_{(T)} \cdot T^{n^{(j)}} \cdot e^{-\frac{1}{T}\cdot\left(\frac{H_f}{\mathcal{R}}\right)^{T=0K}} ,$$

Table II. Stoichiometric mole numbers of equilibrium equations used for calculating speed of sound

Chemical Change	j or ℓ	$\Delta\nu^{(j)}$ or $\Delta\nu^{(\ell)}$
$1/H_2 + 1/2\ Br_2 \rightarrow HBr$	1	0
$1/Br_2 \rightarrow Br$	2	0.5
$1/2\ H_2 \rightarrow H$	3	0.5
$\nu_{H_2}^{(1)} = -0.5$ $\quad \nu_{H}^{(1)} = 0$	$\nu_{Br_2}^{(1)} = -0.5$ $\quad \nu_{Br}^{(1)} = 0$	$\nu_{HBr}^{(1)} = 1$
$\nu_{H_2}^{(2)} = 0$ $\quad \nu_{H}^{(2)} = 0$	$\nu_{Br_2}^{(2)} = -0.5$ $\quad \nu_{Br}^{(2)} = 1$	$\nu_{HBr}^{(2)} = 0$
$\nu_{H_2}^{(3)} = -0.5$ $\quad \nu_{H}^{(3)} = 1$	$\nu_{Br_2}^{(3)} = 0$ $\quad \nu_{Br}^{(3)} = 0$	$\nu_{HBr}^{(3)} = 0$

Table III. Enthalpy changes of equilibrium conditions in reacting hydrogen-bromine mixture

$$\left(\frac{\Delta H}{\mathcal{R}T}\right)^{(1),T} = \left(\frac{H_f}{\mathcal{R}T}\right)_{HBr}^{T} - 1/2\left(\frac{H_f}{\mathcal{R}T}\right)_{H_2}^{T} - 1/2\left(\frac{H_f}{\mathcal{R}T}\right)_{Br_2}^{T}$$

$$\left(\frac{\Delta H}{\mathcal{R}T}\right)^{(2),T} = \left(\frac{H_f}{\mathcal{R}T}\right)_{Br}^{T} - 1/2\left(\frac{H_f}{\mathcal{R}T}\right)_{Br_2}^{T}$$

$$\left(\frac{\Delta H}{\mathcal{R}T}\right)^{(3),T} = \left(\frac{H_f}{\mathcal{R}T}\right)_{H}^{T} - 1/2\left(\frac{H_f}{\mathcal{R}T}\right)_{H_2}^{T}$$

Table IV. Reduced sensible enthalpies, $\left(\frac{H-E_0}{\mathcal{R}T}\right)_i^T$

T (K) \ i	H_2	Br_2	Br	HBr
300	3.425	3.925	2.499	3.489
400	3.436	4.040	2.500	3.494
500	3.452	4.119	2.500	3.499
600	3.464	4.178	2.500	3.509
700	3.474	4.223	2.502	3.523
800	3.484	4.258	2.504	3.543
900	3.495	4.288	2.508	3.566
1000	3.507	4.312	2.513	3.592
1100	3.520	4.332	2.520	3.620
1200	3.534	4.350	2.527	3.648
1300	3.550	4.366	3.534	3.677
1400	3.568	4.380	2.542	3.706
1500	3.587	4.392	2.551	3.734
1600	3.608	4.404	2.559	3.762
1700	3.628	4.414	2.567	3.788
1800	3.650	4.423	2.575	3.814
1900	3.671	4.432	2.583	3.839
2000	3.692	4.440	2.590	3.862
2100	3.714	4.448	2.597	3.885
2200	3.736	4.455	2.604	3.907
2300	3.757	4.462	2.610	3.927
2400	3.778	4.689	2.615	3.947
2500	3.799	4.475	2.620	3.966
2600	3.819	4.481	2.625	3.985
2700	3.839	4.487	2.629	4.002
2800	3.859	4.492	2.633	4.019
2900	3.878	4.498	2.636	4.035
3000	3.897	4.503	2.639	4.051

Table V. Dimensionless specific heats, $\left(\frac{C_p}{\mathcal{R}}\right)_i^T$, of HBr, Br_2, and Br

T (K) \ i	HBr	Br_2	Br
2000	4.3252	4.6000	2.7315
2100	4.3509	4.6055	2.7361
2200	4.3741	4.6111	2.7391
2300	4.3952	4.6166	2.7406
2400	4.4148	4.6222	2.7411
2500	4.4329	4.6277	2.7401
2600	4.4500	4.6327	2.7386
2700	4.4656	4.6383	2.7366
2800	4.4802	4.6438	2.7335
2900	4.4938	4.6488	2.7300
3000	4.5069	4.6544	2.7265

where $a^{(j)}(T)$, a coefficient which depends only slightly on temperature, and $n^{(j)}$, a constant which is closely related to $\Delta\nu^{(j)}$, but may be selected arbitrarily to make the variation of $a^{(j)}$ with T as small as possible. The coefficients $a^{(j)}(T)$ are derived from the rigorously calculated equilibrium constants which have been calculated by the methods of statistical mechanics. Thus we can write the expressions of the equilibrium constants as functions of temp rature in the following forms:

$$K_p^{(H)} = \frac{p_H}{\sqrt{p_{H_2}}} = \left[a^{(H)}(T_L)\right]^{\frac{T_H-T}{100}} \cdot \left[a^{(H)}(T_H)\right]^{\frac{T-T_L}{100}}$$

$$\cdot T^{0.5} \cdot e^{-25982/T}\left[\text{atm}^{0.5}\right], \tag{11}$$

$$K_p^{(Br)} = \frac{p_{Br}}{\sqrt{p_{Br_2}}} = \left[a^{(Br)}(T_L)\right]^{\frac{T_H-T}{100}} \cdot \left[a^{(Br)}(T_H)\right]^{\frac{T-T_L}{100}}$$

$$\cdot T^{0.75} \cdot e^{-11437.66/T}\left[\text{atm}^{0.5}\right], \text{ and} \tag{12}$$

$$K_p^{(HBr)} = \frac{p_{HBr}}{\sqrt{p_{H_2} \cdot p_{Br_2}}} = \left[a^{(HBr)}(T_L)\right]^{\frac{T_H-T}{100}}$$

$$\cdot \left[a^{(HBr)}(T_H)\right]^{\frac{T-T_L}{100}} \cdot e^{-6155.208/T}\left[\text{atm}^{0}\right]. \tag{13}$$

The coefficients $a^{(j)}(T)$ are given in Table VI. The temperature T_L is the nearest integer multiple of 100 below the temperature T.

Table I contains also the Mach numbers based on the frozen equilibrium speed of sound; i.e.,

$$w_{a,r}^{f,eq.} = \sqrt{\gamma_r \frac{\mathcal{R}T_r}{m_r}}, \tag{14}$$

where

$$\gamma_r = \frac{\sum_i \eta_{i,r} \left(\frac{c_p}{\mathcal{R}}\right)_i^{T_r}}{\sum_i \eta_{i,r} \left(\frac{c_p}{\mathcal{R}}\right)_i^{T_r} - 1}.$$

Table VI. Coefficients $a^{(j)}(T)$ for calculating equilibrium constants $K_p^{(j)}(T)$

T (K) \ j	1/2 H_2 ⇌ H $a^{(H)}(T)$	1/2 Br_2 ⇌ Br $a^{(Br)}(T)$	1/2 H_2 + 1/2 Br_2 ⇌ HBr $a^{(HBr)}(T)$
1100	14.038	2.8556	2.9434
1200	14.342	2.7608	2.8665
1300	14.619	2.6703	2.7971
1400	14.853	2.5911	2.7390
1500	15.049	2.5262	2.6908
1600	15.252	2.4574	2.6501
1700	15.428	2.3995	2.6094
1800	15.602	2.3505	2.5758
1900	15.757	2.3031	2.5414
2000	15.863	2.2588	2.5143
2100	16.002	2.2168	2.4892
2200	16.119	2.1780	2.4656
2300	16.211	2.1400	2.4477
2400	16.275	2.1065	2.4276
2500	16.351	2.0772	2.4140
2600	16.405	2.0477	2.3925
2700	16.451	2.0194	2.3820
2800	16.495	1.9892	2.3675
2900	16.543	1.9682	2.3508
3000	16.585	1.9406	2.3385
$n^{(j)}$ =	0.5	0.75	0
$(H_f/\mathcal{R})^{T=0K}$ =	25982 K	11437.66 K	-6155.208 K

$$K_p^{(j)} = a^{(j)}(T) \cdot T^{n^{(j)}} \cdot e^{-1/T(H_f/\mathcal{R})^{T=0K}}$$

$$a^{(j)}(T) = \left[a^{(j)}(T_L)\right]^{\frac{T_H-T}{100}} \cdot \left[a^{(j)}(T_H)\right]^{\frac{T-T_L}{100}}$$

$T = abxy \qquad T_L = ab00 \qquad T_H = T_L + 100$

$$\frac{T_H-T}{100} = 1 - 0.xy \qquad \frac{T-T_L}{100} = 0.xy$$

$1 \le a \le 2$
$0 \le b \le 9$
$0 \le x \le 9$
$0 \le y \le 9$

This Mach number is not 1 for the C.J. detonation because the single pulse rarefaction wave which follows the tail of the detonation wave cannot create a nonequilibrium state in this chemically reacting gas mixture which is assumed to be in complete equilibrium at the tail of the C.J. detonation wave. This fact is shown in Fig. 1 which reveals clearly that the minimum of the w_1 versus T_r curve agrees with the condition $M_{w_r}^{C.J.} = 1$ only when the shifting equilibrium speed of sound is used.

The composition (mole fractions $\eta_{i,r}$) of the detonated gas mixture was calculated by using in addition to the three equilibria, (Eqs. 11, 12, and 13) the condition that $\sum_i \eta_{i,r} = 1$.

An iterative procedure starting with an estimate of $\sqrt{\eta_{H_2}}$ was used to calculate the mole fraction of bromine according to the equation

$$\sqrt{\eta_{Br_2}} = \left[\left[\frac{\sqrt{\eta_{H_2}} \cdot K^{(HBr)} + K^{(Br)}}{2}\right]^2 + 1 - \eta_{H_2} - \eta_H\right]^{0.5} - \frac{\sqrt{\eta_{H_2}} \cdot K^{(HBr)} + K^{(Br)}}{2},$$

which is based on the three equilibrium conditions ($j = 1$, 2, and 3) and the fact that $\sum \eta_i = 1$. The dimensionless equilibrium constants $K^{(Br)}$ and $K^{(H)}$ are obtained by dividing those given by Eq. (11) and Eq. (12) by the square root of the estimated pressure p_r. The accuracy of the estimated mole fraction of molecular hydrogen is determined by evaluating the ratio of total bromine to total hydrogen which, in the present case, should be 1. Hence the iterations are continued with adjusted values of $\sqrt{\eta_{H_2}}$ until

$$100 \cdot \left| \frac{\eta_{Br_2} + \frac{1}{2}\eta_{Br}}{\eta_{H_2} + \frac{1}{2}\eta_H} - 1 \right| < \delta \approx 0.1\% .$$

The equilibrium mole fractions of the gas mixture at the tail of the C.J. detonation are given in the last row of Table VII (also Table VIII). For each of the calculated detonation wave speeds w_1 the conditions of the shocked but unreacted gas were calculated by finding (by an iterative procedure) the pressure p_2 from the Hugoniot equation [Eq. (1)] with assumed temperatures T_2, where now

Table VII. Driver gas (helium at T_4 = 300 K) pressures required to produce normal shock and detonation waves in a one mole hydrogen one mole bromine mixture at T_1 = 313 K and p_1 = 1 atm

Normal Shock without Chemical Change				Detonation (Chemical Equilibrium)		
w_1 (m/s)	p_2 (atm)	u_2 (m/s)	p_4 (atm)	p_r (atm)	u_r (m/s)	p_4 (atm)
649.7	11.10	500.1	27.11			
711.7	13.36	558.5	36.61			
769.0	15.63	611.8	47.71			
930.8*	23.00	760.3	96.04	12.71	404.1	25.81
931.0	23.02	760.4	96.10	12.99	414.1	26.88
939.6	23.48	768.3	99.75	14.65	467.3	33.56
989.3	25.96	813.4	121.81	19.01	585.4	55.00
1197.7	38.34	1002.3	279.17	33.65	876.6	182.13
1480.2	58.88	1257.4	831.42	55.85	1191.9	659.59

*C.J. detonation

$$a = \frac{T_2}{T_1} \text{ (since } \mathcal{M}_2 = \mathcal{M}_1\text{) and } c = \frac{1}{2}\left[\left(\frac{H-E_0}{\mathcal{R}T}\right)^{T_2}_{H_2} + \left(\frac{H-E_0}{\mathcal{R}T}\right)^{T_2}_{Br_2}\right].$$

The accuracy of the assumed T_2 was determined by calculating the wave speed w_1^{calc}:

$$w_1^{calc} = \left[\frac{\left(\frac{p_2}{p_1} - 1\right) R_1 T_1}{1 - \frac{T_2}{T_1} \cdot \frac{p_1}{p_2}}\right]. \qquad (15)$$

The iterations were continued until

$$100 \cdot \left|\frac{w_1^{calc} - w_1}{w_1}\right| < \Delta \simeq 0.1\% .$$

The results of these calculations are included in Table I.

The driver gas (helium at $T_4 = 300$ K) pressures, $p_4^{N.S.}$, which are required to produce normal shock waves of various strength in the unreacted hydrogen-bromine mixture and those required to maintain detonation waves of various strength, $p_4^{det.}$, have been calculated by means of the equation

$$p_4 = \frac{p_3}{\left[1 - \frac{\gamma - 1}{2} \cdot \frac{u_3}{w_{a,4}}\right]^{2\gamma/\gamma-1}} = \frac{p_3}{\left[1 - u_3 \cdot 3.269 \cdot 10^{-4}\right]^8}, \qquad (16)$$

where $p_3 = p_2$ and $u_3 = u_2 = w_1\left(1 - \frac{T_2}{T_1} \cdot \frac{p_1}{p_2}\right)$ for calculating $p_4^{N.S.}$, and $p_3 = p_r$ and $u_3 = u_r = w_1\left(1 - \frac{T_r}{T_1} \cdot \frac{\mathcal{M}_1}{\mathcal{M}_r} \cdot \frac{p_1}{p_r}\right)$ for calculating $p_4^{det.}$. The results of these calculations are listed in Table VII. When the pressure of the shocked but unreacted gas mixture, p_2, and that behind the detonation wave, p_r, are graphically represented as functions of the driver gas pressure (see Fig. 2) it can be seen readily that for a given driver gas pressure, p_4, the pressure behind a detonation wave p_r is higher than p_2 which would prevail if only a normal shock wave in a chemically inert hydrogen-bromine mixture were produced. For a given wave speed, on the other hand, the pressure at the tail of the normal shock wave is higher than that at the tail of the detonation wave as long as the detonation wave is not overdriven to such an extent that the overall chemical change in the reaction zone becomes endothermic. In this case the flow relative to the shock wave would represent a subsonic flow with cooling instead of heating. Similarly, Fig. 3 shows that for a given driver pressure the speed of a detonation wave is much greater than the wave speed which is attained if only a normal shock wave is produced in a chemically inert

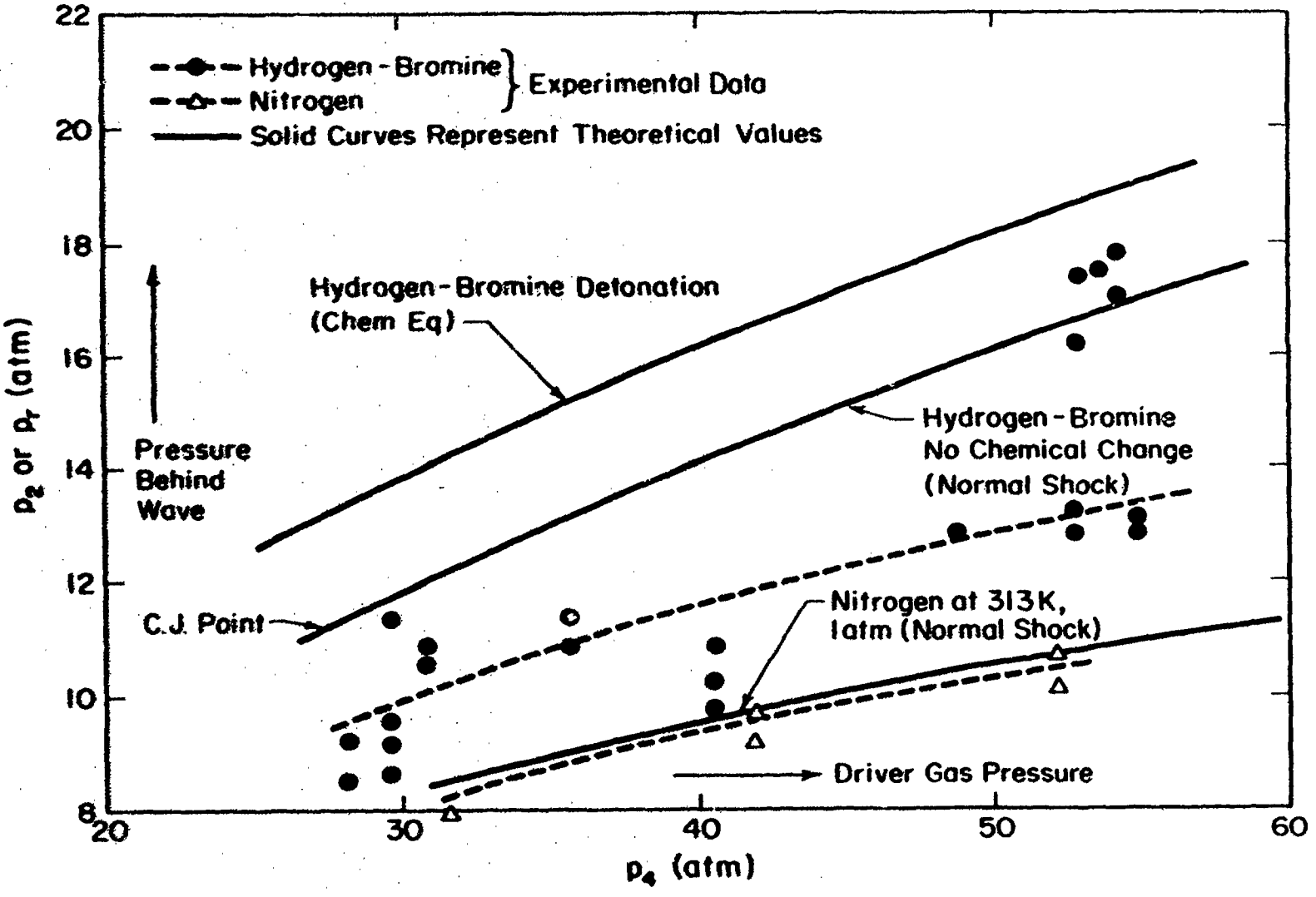

Fig. 2 - Pressures behind normal shock and detonation waves as functions of driver gas pressure

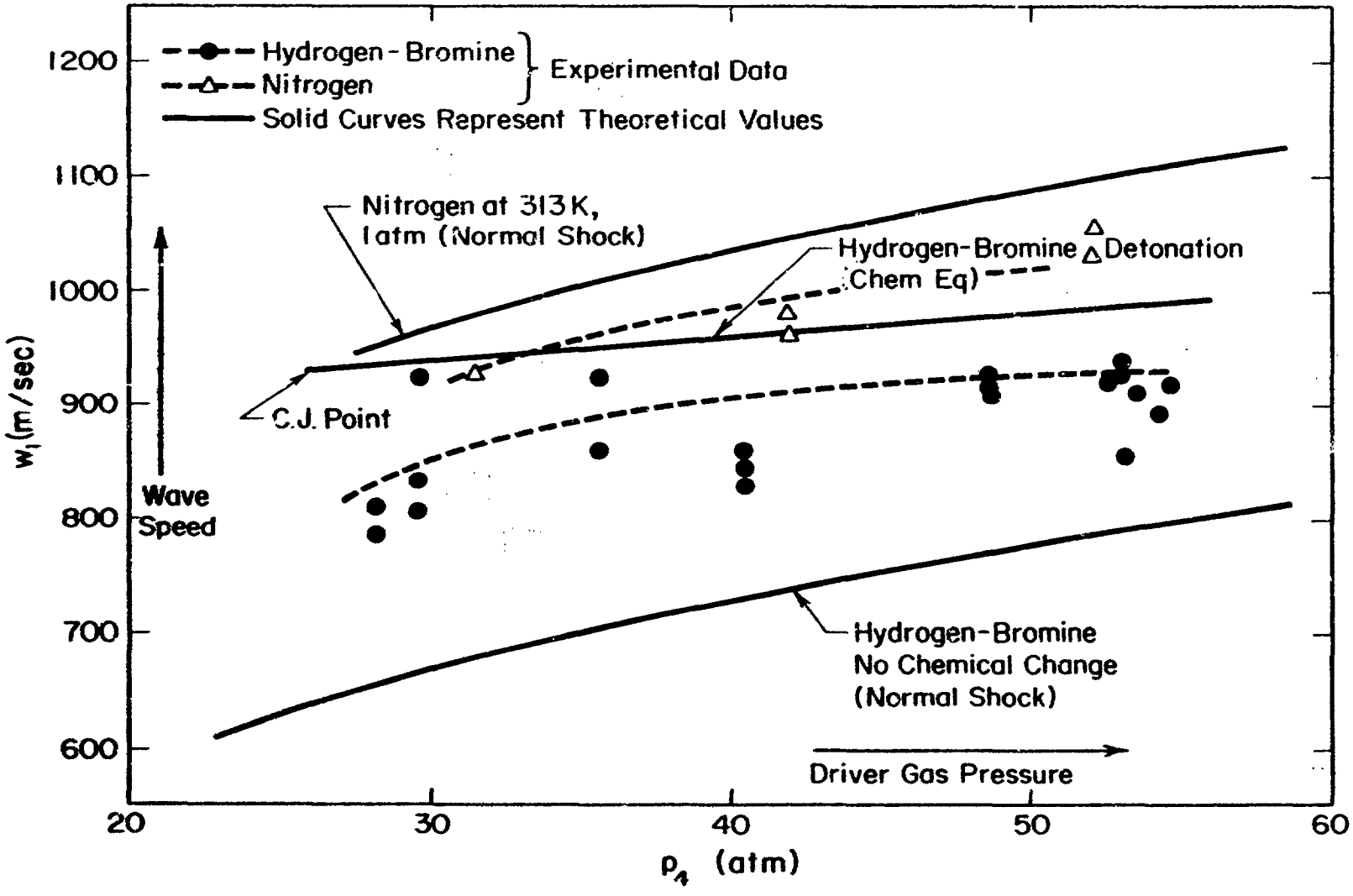

Fig. 3 - Speeds of normal shock and detonation waves as functions of the driver gas pressure

hydrogen-bromine mixture. According to the preceding considerations it is possible to use pressure and wave speed measurements to determine whether a detonation wave or only a normal shock wave was produced in a given experiment with a certain driver gas pressure. Therefore it is not necessary to make measurements of the emission or absorption of radiation of some of the reacting species behind the wave to ascertain the presence of a detonation wave.

2. Estimate of Effect of Intermolecular Forces on Shocked Gas State

Since the real gas effects of hydrogen-bromine mixtures are not known, initial conditions corresponding as closely as possible to those selected for the hydrogen-bromine mixture were used for the real gas calculations to obtain some quantitative data on the real gas effects on the shocked gas parameters. Carbon dioxide was chosen as the equivalent real gas because its critical data are well known and Berthelot's equation was used because it is more realistic than the Van der Waals equation of state and still it yields a relatively simple expression of the real gas enthalpy as a function of temperature and pressure (or specific volume).

The critical temperature of bromine is 575.15 K, whereas that of carbon dioxide is only 304.25 K. The vapor pressure of carbon dioxide reaches 1 atm at 194.65 K. At pressures below that of the triple point ($p = 5.112$ atm with $T = 216.55$ K) carbon dioxide can exist only in the solid phase at any temperature. To make sure that carbon dioxide is in the gaseous state the calculations of the shocked gas conditions in carbon dioxide were made for an initial temperature of 200 K and an initial pressure of 1 atm. The exact value of the critical pressure of bromine is not known. It may be as high as 200 atm, whereas that of carbon dioxide is only 73 atm. In spite of this low value the initial pressure was set at 1 atm to obtain an upper limit of the real gas contribution. The calculations are based on Berthelot's equation of state; i.e.,

$$p = \frac{\Re T}{v - b'} - \frac{a'}{v^2 T}, \tag{17}$$

with

$$a' = \frac{27}{64} (\Re T_c)^2 \cdot \frac{T_c}{p_c} = 135928 \left[\frac{N}{m^2} \cdot \left(\frac{m^3}{kg} \right)^2 \cdot K \right]$$

and

$$b' = 5.46386 \cdot 10^{-4} \left[\frac{m^3}{kg} \right].$$

With this equation the reduced sensible enthalpy as a function of temperature and pressure can be written in the following form:

$$\left(\frac{H-E_0}{\mathcal{R}T}\right)^{T,p} = \left(\frac{H-E_0}{\mathcal{R}T}\right)^{T_1 p=0} + \frac{1}{\frac{v}{b'} - 1} - \frac{3a'}{RvT^2} . \tag{18}$$

The first term on the right hand side of this equation is obtained from tables (such as Jannaf).

According to the energy equation for a normal shock wave the pressure of the shocked gas is

$$p = p_1 \left[\frac{\frac{T}{T_1}\left(\frac{H-E_0}{\mathcal{R}T}\right)^{T_1 p} - \left(\frac{H-E_0}{\mathcal{R}T}\right)^{T_1, p_1}}{\frac{1}{2}\frac{p_1 v_1}{\mathcal{R}T}\left(1 + \frac{v}{v_1}\right)} + 1 \right] . \tag{19}$$

With $T_1 = 200$ K and $p_1 = 1$ atm we obtain, from Eq. (17), $v_1 = 0.354554 \left[\frac{m^3}{kg}\right]$, so that

$$\frac{p_1 v_1}{RT_1} = 0.95081 .$$

The shocked gas parameters (p_2, v_2, u_2) are calculated for given values of the shocked gas temperature T_2 by an iterative procedure. With an assumed value of the specific volume v_2 (which may be obtained by means of the thermally perfect gas relationship) the shocked gas pressure p_2 is calculated by means of Eq. (19) and Eq. (17). If the two values differ, the calculations are repeated with properly adjusted values of v_2 until

$$100 \left| \frac{p_2^{(Eq.19)} - p_2^{(Eq.17)}}{p_2^{(Eq.15)}} \right| < 0.1\% . \tag{20}$$

After a compatible set of p_2, v_2, and T_2 values has been calculated the wave speed is obtained from

$$w_1 = \sqrt{p_1 v_1 \frac{\frac{p_2}{p_1} - 1}{1 - \frac{v_2}{v_1}}} \tag{21}$$

instead of Eq. (3), and the speed of the shocked gas from

$$u_2 = \sqrt{p_1 v_1 \left(\frac{p_2}{p_1} - 1\right)\left(1 - \frac{v_2}{v_1}\right)} . \tag{22}$$

Finally, the helium driver gas pressure, $p_4(T_4 = 300$ K), is calculated from the following equation:

$$p_4 = \frac{p_2}{\left[1 - u_2 \cdot 3.2696 \cdot 10^{-4}\right]^5} \cdot \qquad (23)$$

The results of these calculations are compiled in Table XVI and presented graphically in Figs. 12-16.

3. Calculation of Length of Reaction Zone

It is usually assumed (see Ref. 1, 4, and 5) that a stable detonation wave can be produced in an exothermic system only when, in the flow field behind a normal shock wave passing through this mixture, the rate of energy release is as high as that provided by a reaction mechanism involving chain branching. The rates provided by a simple set of chain reactions without branching are considered to be too slow for maintaining a stable wave. However, the following calculations will show that a stable detonation wave can occur in a one mole hydrogen-one mole bromine mixture even if the reaction mechanism for the formation of hydrogen bromide involves only a simple chain without branching. If it is assumed that the formation of hydrogen bromide behind a shock wave passing through the mixture occurs according to the mechanism established by the classical theory of reaction rates (Ref. 1 and 2), the rate at which hydrogen bromide appears behind the shock wave is

$$\frac{dc_{HBr}}{dt} = \frac{2k^{(2)} \sqrt{\frac{k^{(1)}}{k^{(5)}}} \cdot c_{H_2} \sqrt{c_{Br_2}}}{1 + \frac{k^{(4)}}{k^{(3)}} \cdot \frac{c_{HBr}}{c_{Br_2}}} \text{ (mol/lit·s)} , \qquad (24)$$

where the c_j (c_{HBr}, c_{H_2}, etc.) denote the concentrations in mol/lit. This differential equation follows from the set of reactions tabulated in Table VIII together with the assumption that

$$\frac{dc_H}{dt} = \frac{dc_{Br}}{dt} = 0 .$$

The $k^{(j)}$ are the so-called reaction rate constants which are functions of temperature. According to experiments (Ref. 1) the reaction rate constant $k^{(2)}$ is given by the following equation:

$$k^{(2)} = 4.55 \times 10^{10} \times e^{-8863/T} \text{ (lit/mol·s)} . \qquad (25)$$

The ratio of $k^{(1)}$ to $k^{(5)}$ can be expressed terms of the equilibrium constant, $K_p^{(Br)}$, for dissociating molecular bromine as long as the assumption that the rate of atomic bromine formation [reaction (1)] is equal to the

Table V II. Reaction mechanism of HBr formation

Reaction Number (j)	Formula of Reaction	Enthalpy Change of Reaction ($J/kmol \times 10^6$)	Rate of Reaction
(1)	$Br_2 + M = 2Br + M$	- 189.2	$(Br) = k^{(1)}(Br_2)(M)$
(2)	$Br + H_2 = HBr + H$	- 68.66	$(HBr) = k^{(2)}(Br)(H_2)$
(3)	$H + Br_2 = HBr + Br$	169.6	$(HBr) = k^{(3)}(H)(Br_2)$
(4)	$H + HBr = H_2 + Br$	68.66	$(Br) = k^{(4)}(H)(HBr)$
(5)	$2Br + M = Br_2 + M$	189.2	$(Br_2) = k^{(5)}(Br)^2(M)$

recombination rate of atomic bromine [reaction (5)] applies not only to near equilibrium conditions but also to all other conditions. Hence we can write

$$k^{(1)} \cdot c_{Br_2} = k^{(5)} \cdot c_{Br}^2 \ ;$$

with

$$c_i = \frac{p_i}{\mathcal{R}T} = \frac{p}{\mathcal{R}T} \cdot \eta_i \ ,$$

we obtain

$$\sqrt{\frac{k^{(1)}}{k^{(5)}}} = \frac{c_{Br}}{\sqrt{c_{Br_2}}} \equiv K_c^{(Br)} = \frac{1}{\sqrt{\mathcal{R}T}} \cdot \frac{p_{Br}}{\sqrt{p_{Br_2}}} \equiv \frac{K_p^{(Br)}}{\sqrt{\mathcal{R}T}} \ .$$

Since reactions (3) and (4) are quite exothermic, their activation energies are quite small. For this reason the ratio $k^{(4)}/k^{(3)}$ is practically independent of temperature and according to experiments we have $k^{(4)}/k^{(3)} = 0.12$ over a moderate range of temperatures. When in the rate expression Eq. (6) some of the concentrations are replaced by the mole fractions and the above expressions for $k^{(2)}$, $k^{(1)}/k^{(5)}$, and $k^{(4)}/k^{(3)}$ are substituted, we obtain

$$\frac{dc_{HBr}}{dt} = \frac{9.1 \cdot 10^{10} \cdot e^{-8863/T} \cdot K_p^{(Br)} \cdot p^{1.5} \cdot \eta_{H_2} \cdot \sqrt{\eta_{Br_2}}}{(\mathcal{R}T)^2 \left[1 + 0.12 \cdot \frac{\eta_{HBr}}{\eta_{Br_2}}\right]} \ ,$$

where

$$\mathcal{R} = 0.082056 \ \text{lit} \cdot \text{atm/mol} \cdot \text{K} \ .$$

Upon substitution of the expression for the equilibrium constant, Eq. (12), and solving for dt, we arrive at

$$dt = \frac{\left[1 + 0.12 \frac{\eta_{HBr}}{\eta_{Br_2}}\right] \cdot T^{1.25} \cdot e^{20300.66/T} \cdot dc_{HBr}}{1.35 \cdot 10^{13} \cdot \eta_{H_2} \cdot \sqrt{\eta_{Br_2}} \cdot a^{(Br)}(T) \cdot p^{1.5}} \ . \qquad (26)$$

Since the shocked and reacting gas mixture travels relative to the wave front with the speed w which ranges from w_2 at the tail of the shock wave to w_r at the tail of the detonation wave, we have, using the continuity equation and the equation of state,

$$dL_r = w \cdot dt = w_1^{C.J.} \cdot \frac{\nu}{\nu_1} \cdot dt \ ,$$

and thus for the total length of the reaction zone, L_r,

$$L_r = w_1^{C.J.} \cdot \int_2^r \frac{\nu}{\nu_1} dt = w_1^{C.J.} \cdot \int_2^r \frac{T}{T_1} \cdot \frac{\mathcal{M}_1}{\mathcal{M}} \cdot \frac{p_1}{p} \cdot dt \ .$$

Upon substitution of Eq. (26) into this expression we obtain

$$L_r = \frac{w_1^{C.J.} \cdot \mathcal{M}_1 p_1}{1.35 \cdot 10^{13} \cdot T_1} \cdot \int_2^r \frac{\left[1 + 0.12 \frac{\eta_{HBr}}{\eta_{Br_2}}\right] \cdot T^{2.25} \cdot e^{20300.66/T} \cdot dc_{HBr}}{\eta_{H_2} \cdot \sqrt{\eta_{Br_2}} \cdot \mathcal{M} \cdot a^{(Br)}(T) \cdot p^{2.5}}$$

or

$$\frac{dL_r}{dc_{HBr}} = 1.78 \cdot 10^{-8} \cdot \frac{\left[1 + 0.12 \frac{\eta_{HBr}}{\eta_{Br_2}}\right] \cdot T^{2.25} \cdot e^{20300.66/T}}{\eta_{H_2} \cdot \sqrt{\eta_{Br_2}} \cdot \mathcal{M} \cdot a^{(Br)}(T) \cdot p^{2.5}} \ (\text{lit/mol·mm}) \ , \quad (27$$

since $w_1^{C.J.} = 930805(\text{mm/s})$, $\mathcal{M}_1 = 80.924$ (kg/kmol), $p_1 = 1$ atm, and $T_1 = 313$ K. The molecular mass, $\mathcal{M} = \sum \eta_i \mathcal{M}_i$, is a function of the gas composition (see Tables IX and X). Incremental increases of the reaction zone (ΔL_r) can be calculated by means of Eq. (27) when, for the progress of the reaction which can be expressed in terms of the independent variable η_{HBr}, the corresponding mole fractions of hydrogen, η_{H_2}, and bromine, η_{Br_2}, are known. For a given composition of the gas the corresponding temperature, T, and pressure, p, are calculated by means of the Hugoniot relationship [Eq. (1)] and the condition that the wave speed [Eq. (3)] is $w_1^{C.J.} = 930805(\text{mm/s})$. At the tail of the normal shock wave, at which, according to the assumption made in this analysis, $\eta_{HBr} = \eta_{Br} = \eta_H = 0$ and $\eta_{H_2} = \eta_{Br_2} = 0.5$, the composition of the gas mixture changes from its non-equilibrium state to the equilibrium composition at the end of the reaction zone (= tail of detonation wave). Since pressure and temperature also vary and the reaction zone length is not known, it is not possible to calculate the composition anywhere in this region. However, for assumed profiles of the atomic bromine and atomic hydrogen mole fraction as functions of the mole fraction of hydrogen bromide, which is used to represent the progress of the reaction, it is possible to calculate the length of the reaction zone by an iteration procedure and numerical integration. Using the simple linear relationships

Table IX. Variation of properties in reaction zone of stable detonation wave $\left(w_1^{C.J.} = 930805 \text{ mm/s}\right)$; Profile No. 1, $c_i = \eta_i \cdot \frac{p}{\mathfrak{M}T}$ [mol/lit]

c_{HBr} / η_{HBr}	c_{H_2} / η_{H_2}	c_{Br_2} / η_{Br_2}	c_H / η_H	c_{Br} / η_{Br}	T (K)	p (atm)	$\mathfrak{M}$ (kg/kmol)	L_r (mm)
0.0 0.0	0.10623 0.5	0.10623 0.5	0.0 0.0	0.0 0.0	1319.6	23.006	80.924	0.0
0.01897 0.1	0.08488 0.44748	0.08393 0.44249	$5.6906 \cdot 10^{-6}$ 0.00003	$1.8969 \cdot 10^{-3}$ 0.01	1439	22.398	80.518	0.06441
0.03402 0.2	0.06718 0.39496	0.06549 0.38499	1.0676-5 0.00006	3.4021-3 0.02	1556	21.719	80.112	0.09280
0.04590 0.3	0.05240 0.34243	0.05011 0.32748	1.3771-5 0.00009	4.5903-3 0.03	1671.3	20.984	79.707	0.10629
0.05513 0.4	0.03995 0.28991	0.03721 0.26997	1.6538-5 0.00012	5.5128-3 0.04	1784	20.175	79.301	0.11372
0.06198 0.5	0.02942 0.23739	0.02633 0.21246	1.8593-5 0.00015	6.1977-3 0.05	1893	19.254	78.895	0.11884
0.06668 0.6	0.02054 0.18487	0.01722 0.15496	2.0001-5 0.00018	6.6669-3 0.06	1997	18.208	78.489	0.12294
0.06893 0.7	0.01303 0.13234	0.00960 0.09745	2.0679-5 0.00021	6.8931-3 0.07	2091	16.896	78.083	0.12622
0.06660 0.8	0.00664 0.07982	0.00332 0.03994	1.9979-5 0.00024	6.6595-3 0.08	2169	14.816	77.663	0.13998
0.06159 0.85673	0.00361 0.05019	0.00056 0.00784	1.9411-5 0.00027	6.1087-3 0.08497	2193	12.701	77.475	0.73333

Table X. Variation of properties in reaction zone of stable detonation wave $\left(w_1^{C.J.} = 930805 \text{ mm/s}\right)$; Profile No. 2, $c_i = \eta_i \frac{p_1}{\mathcal{R}T}$ [mol/lit]

c_{HBr} / η_{HBr}	c_{H_2} / η_{H_2}	c_{Br_2} / η_{Br_2}	c_H / η_H	c_{Br} / η_{Br}	T (K)	p (atm)	$\mathfrak{M}$ (kg/kmol)	L_r (mm)
0.0 0.0	1.0623-1 0.5	1.0623-1 0.5	0.0 0.0	0.0 0.0	1319.6	23.006	80.924	0.0
1.854-2 0.1	8.344-2 0.44998	8.343-2 0.44995	4.057-8 0.00000022	1.2813-5 0.0000691	1464.7	22.286	80.921	0.05920
3.265-2 0.2	6.530-2 0.39995	6.528-2 0.39986	9.711-8 0.00000059	3.0692-5 0.0001880	1606.2	21.517	80.916	0.07769
4.337-2 0.3	5.058-2 0.34987	5.055-2 0.34962	2.3377-7 0.00000162	7.3865-5 0.0005109	1743.5	20.684	80.904	0.08540
5.148-2 0.4	3.857-2 0.29965	3.848-2 0.29896	5.6570-7 0.00000440	2.4309-4 0.0018887	1874.0	19.792	80.908	0.08949
5.725-2 0.5	2.851-2 0.24905	2.830-2 0.24717	1.3679-6 0.00001195	4.3224-4 0.0037753	1997.2	18.763	80.771	0.09207
6.125-2 0.6	2.015-2 0.19741	1.963-2 0.19230	3.3150-6 0.0000324 8	1.0496-3 0.0102824	2102.6	17.611	80.509	0.09409
6.395-2 0.7	1.306-2 0.14296	1.179-2 0.12906	8.0648-6 0.00008828	2.5485-3 0.0278962	2174.0	16.297	79.792	0.09636
6.718-2 0.8	6.791-3 0.08086	3.617-3 0.04307	2.0152-5 0.00023997	6.3600-3 0.0758296	2170.4	14.956	77.846	0.11209
6.159-2 0.85673	3.608-3 0.05019	5.636-4 0.00784	1.9411-5 0.00026892	6.1087-3 0.0849728	2153.0	12.701	77.475	0.77125

$$\left.\begin{aligned} \eta_{Br} &= 0.1\eta_{HBr} \\ \text{and} \qquad & \\ \eta_{H} &= 3 \cdot 10^{-4}\eta_{HBr} \end{aligned}\right\} \text{ for the range } 0 \leq \eta_{HBr} \leq 0.8 ,$$

we obtain for a one mole hydrogen--one mole bromine mixture

$$\eta_{Br_2} = 0.5 - 0.575075 \cdot \eta_{HBr} , \quad 0 \leq \eta_{HBr} \leq 0.8$$

and

$$\eta_{H_2} = 0.5 - 0.525225\eta_{HBr} , \quad 0 \leq \eta_{HBr} \leq 0.8 .$$

These relationships were chosen to produce the equilibrium composition at the tail of detonation wave ($\eta_{HBr} = 0.85673$) as closely as possible. The equilibrium mole fractions were always used to calculate dL/dc_{HBr} at the tail of the wave.

To determine the influence of the arbitrarily selected profiles on the length of the reaction zone a second profile was chosen with an exponential relationship between the mole fractions of the atoms (η_{Br} and η_{H}) and that of the hydrogen bromide as follows:

$$\left.\begin{aligned} \eta_{Br} &= 2.5438 \cdot 10^{-5} \cdot e^{10\cdot\eta_{HBr}} \\ \text{and} \qquad & \\ \eta_{H} &= 8.05 \cdot 10^{-8} \cdot e^{10\cdot\eta_{HBr}} \end{aligned}\right\} \text{ for the same range of values as used for profile No. 1.}$$

With these relationships we obtain

$$\eta_{Br_2} = 0.5\left[1 - \eta_{HBr} - 3.819725 \cdot 10^{-5} \cdot e^{10\cdot\eta_{HBr}}\right]$$

and

$$\eta_{H_2} = 0.5\left[1 - \eta_{HBr} - 1.283975 \cdot 10^{-5} \cdot e^{10\cdot\eta_{HBr}}\right] .$$

The composition profiles obtained with these relationships are tabulated in Tables IX and X for arbitrarily selected values of η_{HBr}. The molecular mass of the partially reacted gas mixture is calculated as $\mathfrak{M} = \sum_i \eta_i \mathfrak{M}_i$. With an estimated value of the temperature $T(T_2 < T < T_r)$ the corresponding pressure in the wave is calculated according to the

Hugoniot equation [Eq. (1)]. With these values the wave speed w_1^{calc} can be calculated according to Eq. (3). When w_1^{calc} does not agree with that of the stable detonation wave $\left(w_1^{C.J.} = 930805 \text{ mm/s}\right)$, the calculations must be repeated with an adjusted value of the estimated temperature, T, until satisfactory agreement is reached. After the correct values of $\mathcal{M}$, p, and T have been calculated for a number of η_{HBr}, values the corresponding dL_r/dc_{HBr} values can be calculated by means of Eq. (27). The length of the reaction zone, L_r, is then calculated by means of the following simplified summation process:

$$L_r = \frac{1}{2} \sum_{x=0}^{9} \left[\left(\frac{dL_r}{dc_{HBr}} \right)_x + \left(\frac{dL_r}{dc_{HBr}} \right)_{x+1} \right] \cdot \left[\left(c_{HBr} \right)_{x+1} - \left(c_{HBr} \right)_x \right]. \qquad (28)$$

The more rigorous numerical integration of the $\frac{dL_r}{dc_{HBr}} - c_{HBr}$ relationship will practically lead to the same result as can be seen in Fig. 4. Finally, to make sure that the assumed concentration profiles do not involve any spontaneous entropy decreases, the corresponding entropy profiles through the wave have been calculated according to the equation

$$\frac{s}{R_1} = \frac{\mathcal{M}_1}{\mathcal{M}} \left[\sum_i \eta_i \left(\frac{S^{p=1}}{\mathcal{R}} \right)_i^T - \sum_i \eta_i \ln \eta_i - \ln p \right], \qquad (29)$$

where

$$\left(\frac{S^{p=1}}{\mathcal{R}} \right)_i^T = \ln T \left\{ \frac{T_H - T}{100} \left[\frac{\left(\frac{S^{p=1}}{\mathcal{R}} \right)}{\ln T} \right]_i^{T_L} + \frac{T - T_L}{100} \left[\frac{\left(\frac{S^{p=1}}{\mathcal{R}} \right)}{\ln T} \right]_i^{T_H} \right\}. \qquad (30)$$

The results of these calculations are given in Tables XI and XII and they are shown graphically in Figs. 5-7.

The thermodynamic functions as used in all preceding calculations have been derived from the Jannaf Tables and are compiled in Tables IV, V, VI, XIII, and XIV.

C. EXPERIMENTAL INVESTIGATION

1. Description of Apparatus and Experimental Procedure

Because of the very low flame speeds of hydrogen-bromine mixtures (Ref. 3), it was not expected that detonation waves in hydrogen-bromine mixtures can be established by simple spark ignition leading to the transition from deflagration to detonation. However, a series of experiments

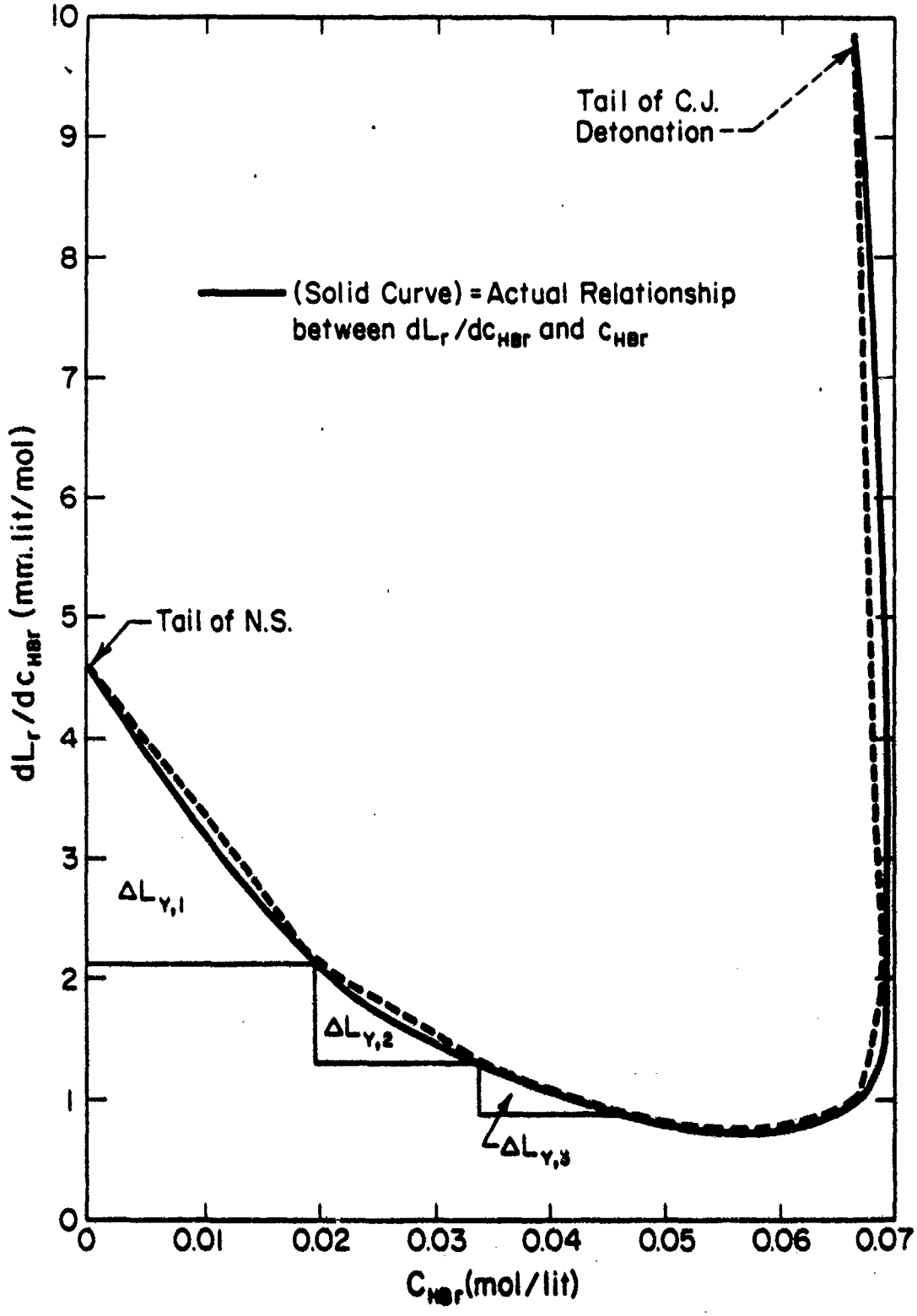

Fig. 4 - Calculation of reaction zone length (Profile No. 1)

Table XI. Reaction zone length and entropy variation for the C.J. detonation wave in a 1 mole hydrogen - 1 mole bromine mixture; Profile No. 1

η_{HBr}	c_{HBr} (mole/lit)	$\frac{dL_r}{dc_{HBr}}$ (mm·mol/lit)	L_r (mm)	S/R_1
0.0	0.0	4.6516	—	26.1437
0.1	1.8968-2	2.1395	0.06441	26.9691
0.2	3.4021-2	1.3974	0.09280	27.7105
0.3	4.5903-2	0.87395	0.10629	28.1404
0.4	5.5127-2	0.73694	0.11372	28.6058
0.5	6.1976-2	0.75724	0.11884	29.0059
0.6	6.6676-2	0.98961	0.12294	29.3424
0.7	6.8933-2	1.91936	0.12622	29.6109
0.8	6.6596-2	9.8533	0.13998	29.8274
0.85673	6.1592-2	227.30	0.73333	29.8375

Table XII. Reaction zone length and entropy variation for the C.J. detonation wave in a 1 mole hydrogen - 1 mole bromine mixture; Profile No. 2

η_{HBr}	c_{HBr} (mole/lit)	$\frac{dL_r}{dc_{HBr}}$ (mm·mol/lit)	L_r (mm)	S/R_1
0.0	0.0	4.6516	—	26.1437
0.1	1.854-2	1.7382	0.05920	26.9435
0.2	3.265-2	0.8833	0.07769	27.5486
0.3	4.337-2	0.5551	0.08540	28.0557
0.4	5.148-2	0.4523	0.08949	28.4867
0.5	5.725-2	0.4445	0.09207	28.8619
0.6	6.125-2	0.5686	0.09409	29.1942
0.7	6.395-2	1.1071	0.09636	29.5024
0.8	6.718-2	8.6206	0.11209	29.7889
0.85673	6.1592-2	227.30	0.77125	29.8375

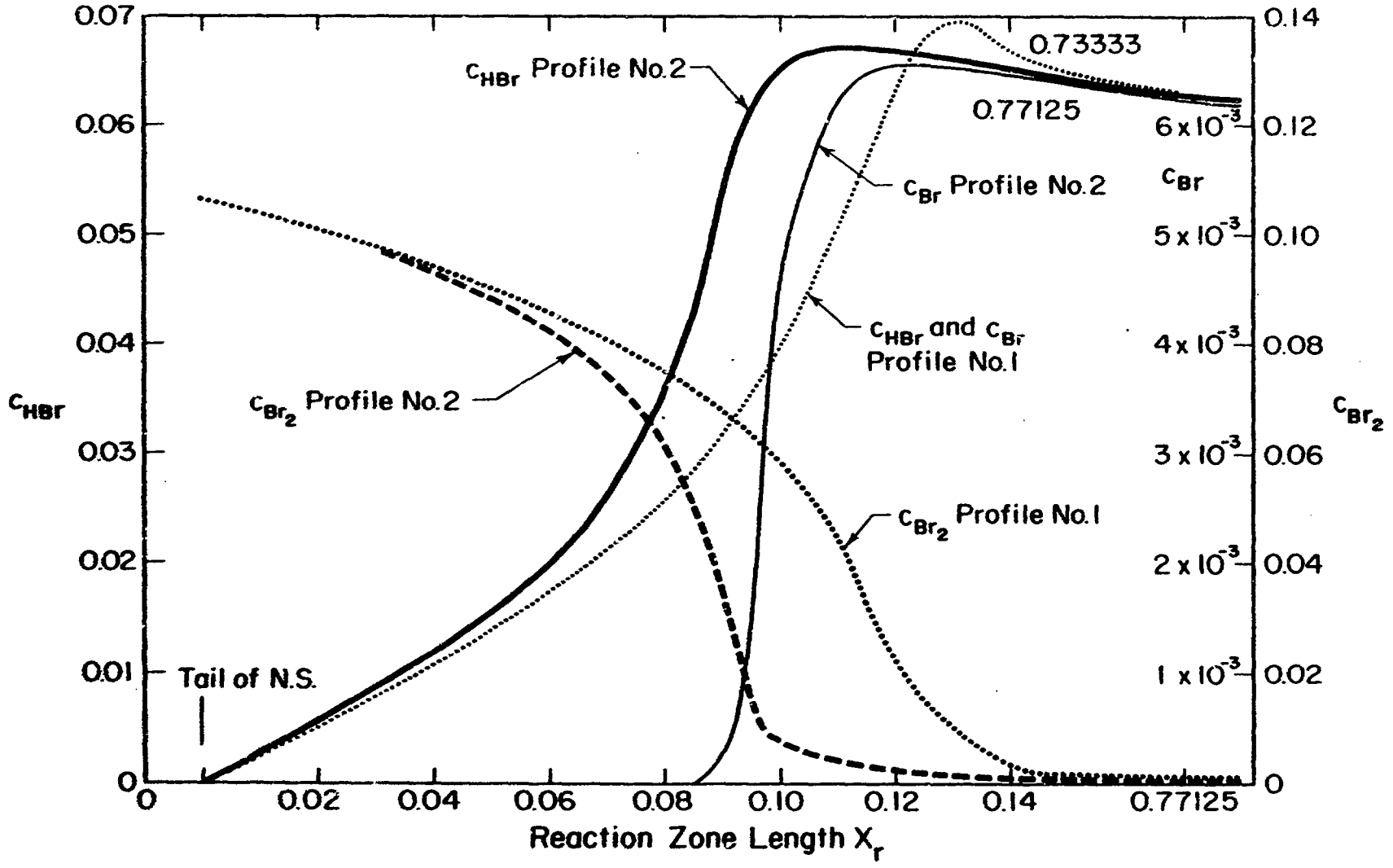

Fig. 5 - Concentration profiles of Br_2, HBr, and Br in reaction zone of a detonation wave in a 1 mole hydrogen-1 mole bromine mixture

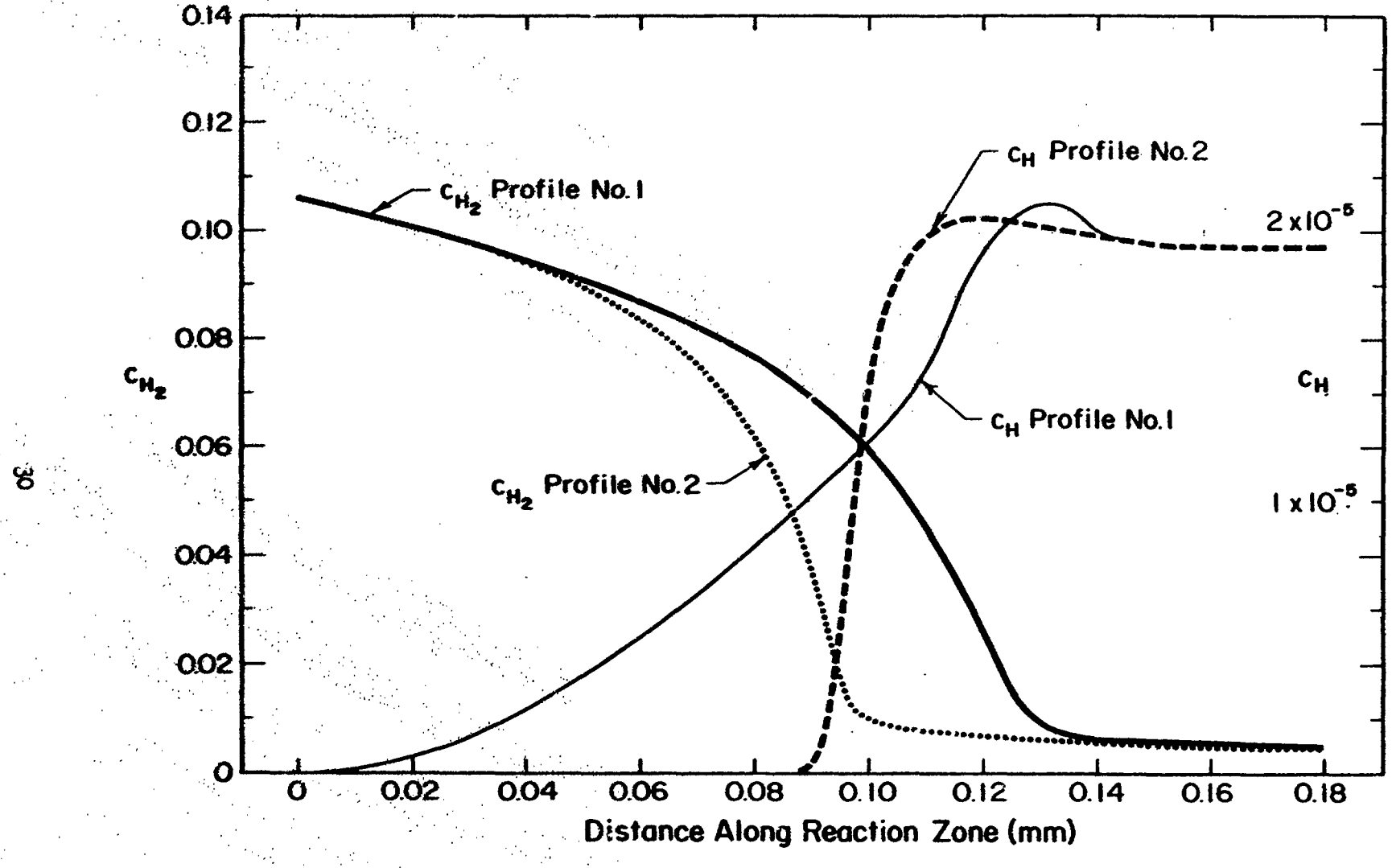

Fig. 6 - Concentration profiles of H_2 and H in the reaction zone of a detonation wave in a 1 mole hydrogen-1 mole bromine mixture

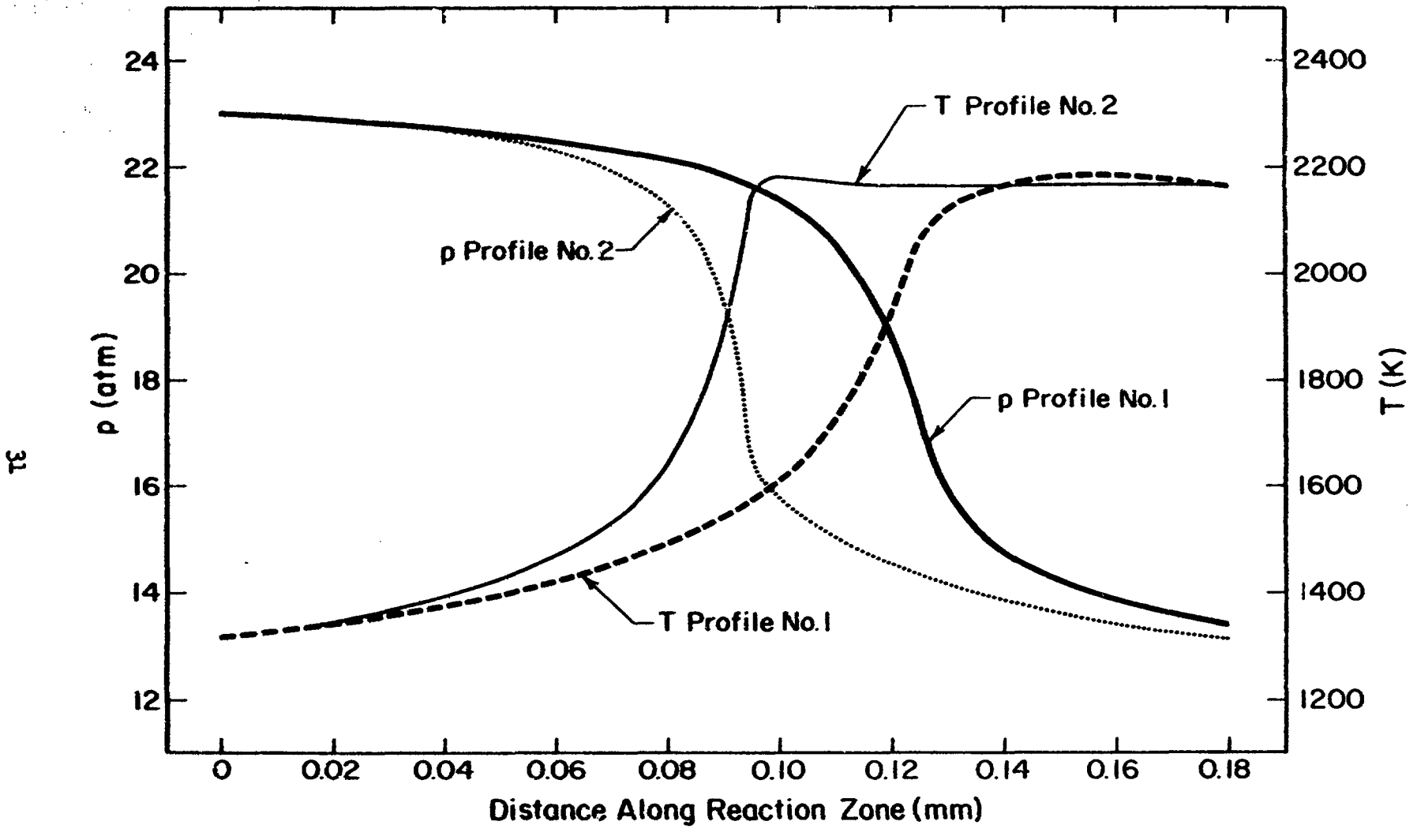

Fig. 7 - Pressure and temperature profiles in the reaction zone of a detonation wave in a 1 mole hydrogen-1 mole bromine mixture

Table XIII. Dimensionless entropies of Br_2, Br, and HBr, $\left(S^{p=1}/\mathcal{R}\right)_i^T$

T (K)	Br_2	Br	HBr
1300	36.1011	24.7618	29.2672
1400	36.4393	24.9581	29.5697
1500	36.7543	25.1418	29.8545
1600	37.0497	25.3154	30.1237
1700	37.3270	25.4789	30.3794
1800	37.5891	25.6339	30.6224
1900	37.8377	25.7809	30.8539
2000	38.0732	25.9208	31.0748
2100	38.2977	26.0546	31.2867
2200	38.5121	26.1820	31.4895

Table XIV. Temperature coefficients of entropies of Br_2, Br, and HBr, $\left[\frac{\left(S^{p=1}/\mathcal{R}\right)}{\ell n T}\right]_i^T$

T (K)	Br_2	Br	HBr
1300	5.03494	3.45348	4.08183
1400	5.03011	3.44524	4.08183
1500	5.02573	3.43785	4.08226
6100	5.02181	3.43131	4.08304
1700	5.01815	3.42433	4.08414
1800	5.01487	3.41989	4.08542
1900	5.01188	3.41486	4.08682
2000	5.00904	3.41022	4.08830
2100	5.00643	3.40597	4.08993
2200	5.00403	3.40193	4.09156

was carried out to investigate whether there is at least an indication of some flame acceleration. These experiments are rather difficult to execute because (1) to obtain mixtures containing sufficient bromine, moderately elevated temperatures have to be used because of the low vapor pressure of bromine at room temperatures; and (2) extremely long ducts are required to obtain conclusive results because the flame propagation rates of hydrogen-bromine mixtures are only of the order of 12 to 14 cm/s (Ref. 3).

A series of experiments in 3 m long, 3 cm I.D. glass tubes clearly revealed that the flames of these mixtures do not accelerate measurably. Therefore a shock tube of stainless steel was used to find out whether a C.J. detonation can be produced in hydrogen-bromine mixtures by shock ignition. Both the driver and the driven section of the shock tube were 6 m long and had an inside diameter of 7.5 cm. Helium was used as the driver gas. A schematic view of the shock tube is given in Fig. 8. The hydrogen-bromine mixture was produced by bubbling hydrogen gas slowly through liquid bromine contained in a glass wash-bottle. The liquid bromine was held at a temperature of 313 K because at this temperature the bromine vapor pressure is sufficiently high to form a 1 mole bromine-1 mole hydrogen mixture in the gaseous phase. To avoid condensation of the bromine vapor, all lines and the driven section carrying the hydrogen-bromine mixture had to be heated to 313 K. The pressure of the hydrogen-bromine mixture in the driven gas section of the shock tube was one atmosphere in all experiments. To obtain the desired driver pressures the strength of the burst diaphragms was properly adjusted by using various numbers of 0.125 mm thick mylar sheets. It would have been preferable to use single sheets of the required thickness but, unfortunately, mylar sheets of the right strength were not available.

After each experiment the products of the reacted gas mixture leaving the shock tube through the vent line were inspected carefully for the presence of unreacted bromine. At the driver gas pressures employed in these experiments the reaction products never contained any detectable quantity of bromine. To remove the hydrogen bromide from the shock tube as completely as possible the shock tube was purged with dry air for 15 minutes and then evacuated before a fresh mixture of hydrogen and bromine was introduced. The results of all measurements are compiled in Table XV.

2. Instrumentation and Calibration

The wave speeds, and the pressures behind the wave, were measured by means of quartz crystal transducers (Kistler) which were mounted in such a manner that the inner wall of the tube remained absolutely smooth. The output of the transducers was displayed on the screen of a Tektronic type 555 dual-beam oscilloscope and the traces were recorded photographically on Polaroid paper. The pressure transducers were calibrated statically and dynamically. For the dynamic tests the driven section of the shock tube was filled with nitrogen at 1 atm and 313 K. The results of this calibration are included in Figs. 2 and 3. All measurements were made at two locations of the driven section of the shock tube. Several

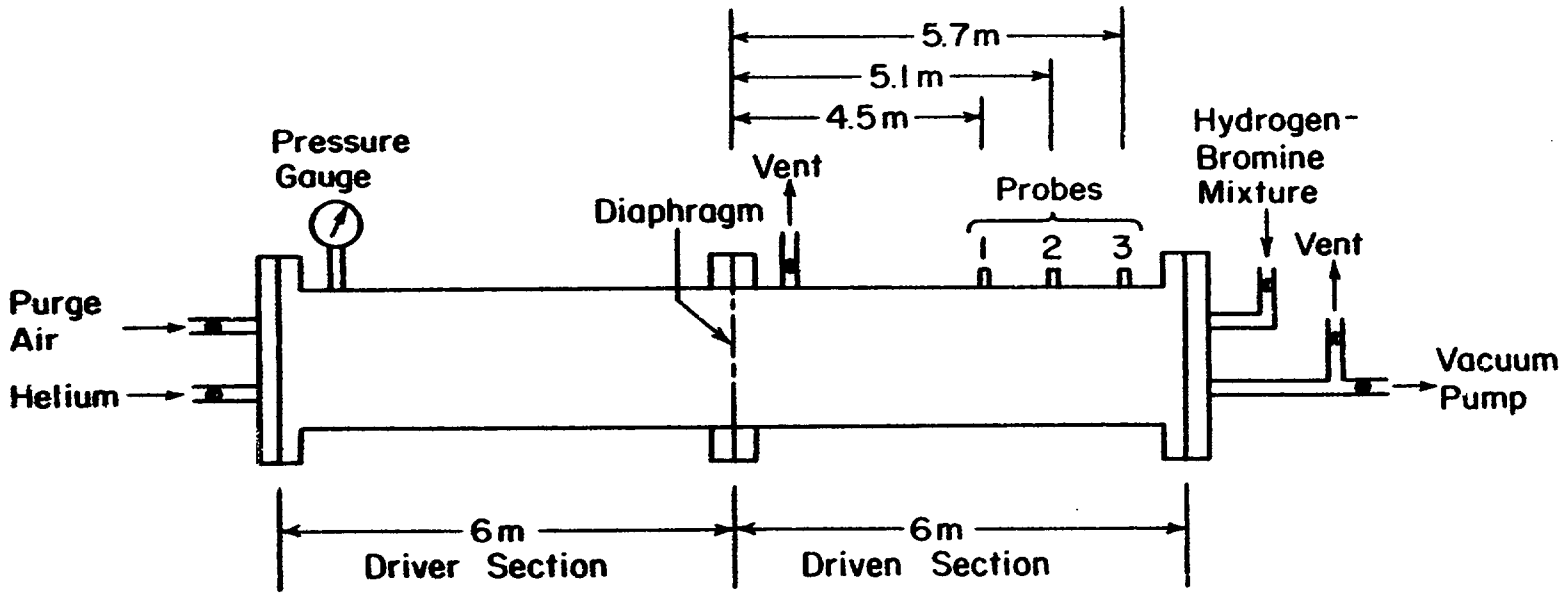

Fig. 8 - Schematic view of shock tube

Table XV. Pressures behind wave and wave speeds measured in the 6 m long driven section of helium driven shock tube (H_2 - Br_2, T = 313 K, p = 1 atm)

	Pressure of Helium at the Instant of Diaphragm Rupture	Location of Transducer	Pressure Behind Incident Wave p_r (atm)	Speed of Wave w_1 (m/s)
1	53.10	3	16.00	921.50
2	53.10	3	16.00	851.30
		2	17.31	952.20
3	54.50	3	17.00	895.50
		2	17.70	895.50
4	53.80	3	17.31	914.40
5	54.85	2	12.85	918.55
		3	13.09	918.55
6	52.80	2	12.85	921.17
		3	13.26	923.08
7	48.72	2	12.91	921.17
		3	12.85	909.09
8	48.72	2	12.85	921.66
9	48.72	2	—	915.12
		3	12.85	916.03
10	40.54	2	—	860.22
		3	10.84	827.59
11	40.54	2	9.27	827.13
		3	10.24	845.07
12	35.76	2	10.84	806.45
		3	11.35	923.08
13	30.99	2	10.56	878.97
		3	10.88	887.57
14	29.63	2	8.65	806.45
		3	11.35	923.08
15	29.63	2	9.17	806.45
		3	9.52	833.33
16	28.27	2	8.49	786.78
		3	9.21	810.81

experiments were made for each driver gas pressure. Two typical oscillograph traces of the wave speed and the pressure of a stable detonation wave are shown in Figs. 9 and 10.

D. DISCUSSION OF RESULTS AND CONCLUSIONS

Since the experimentally determined wave speeds and the pressures behand the wave, as shown in Table XV, agree quite satisfactorily with the theoretical values shown in Table I, it can be concluded that stable detonation waves can be produced in hydrogen-bromine mixtures. That the observed wave speeds are those of detonation waves and not of normal shock waves propagating through the unreacted hydrogen-bromine mixture follows from a comparison of the experimental data with those derived from the theoretical calculations as shown in Figs. 2 and 3. According to Fig. 3, for a driver gas pressure of 53 atm the speed of a shock wave passing through an unreacted 1 mole hydrogen - 1 mole bromine mixture would be 793 m/s, whereas the theoretical speed of a detonation wave is 985 m/s as long as no attenuation of this slightly overdriven wave has occurred. In view of these data it is obvious that the observed wave speed of 915 m/s is that of a detonation wave. At a driver pressure of 30 atm the average value of the observed wave speeds is in even better agreement with the theoretically calculated speed of a detonation wave. It is generally true for all detonable mixtures that experimentally determined detonation wave speeds are smaller than the theoretical values. As will be shown below, the reason for the somewhat larger difference between experimental and theoretical values in hydrogen-bromine mixtures may be caused by the slow rate at which hydrogen bromide is formed at the tail of the detonation wave. Furthermore, the relatively large difference between measured and theoretical speed of the higher driver gas pressures may be caused by an attenuation of the wave in the 7.5 cm I.D. tube. At driver pressures near 30 atm some experimentally determined wave speeds agree quite well with the theoretically calculated values, although in some cases the measured values are quite low particularly at driver pressures below 30 atm. This behavior may be due to the rather rapid increase of $\frac{dL_r}{dc_{HBr}}$ (see Fig. 11) at the tail of the shock wave ($\eta_{HBr} = 0$) when lower driver gas pressures are used. The relationship between $\left(\frac{dL_r}{dc_{HBr}}\right)\eta_{HBr} = 0$ and driver gas pressure, p_4, is shown in Fig. 11, which also shows the relationship between the temperature at the tail of a normal shock wave passing through the hydrogen-bromine mixture (T_2) and the driver gas pressure (p_4). According to these calculations, it can be concluded that ignition occurred in all experiments since driver gas pressures lower than 20 atm have not been used. However, it appears quite certain that the large values of $\left(\frac{dL_r}{dc_{HBr}}\right)\eta_{HBr} = 0$ at these low driver gas pressures prevent the formation of a detonation wave in the mixture. Finally, the fact that the observed speeds of shock waves generated in nitrogen are also approximately 5%

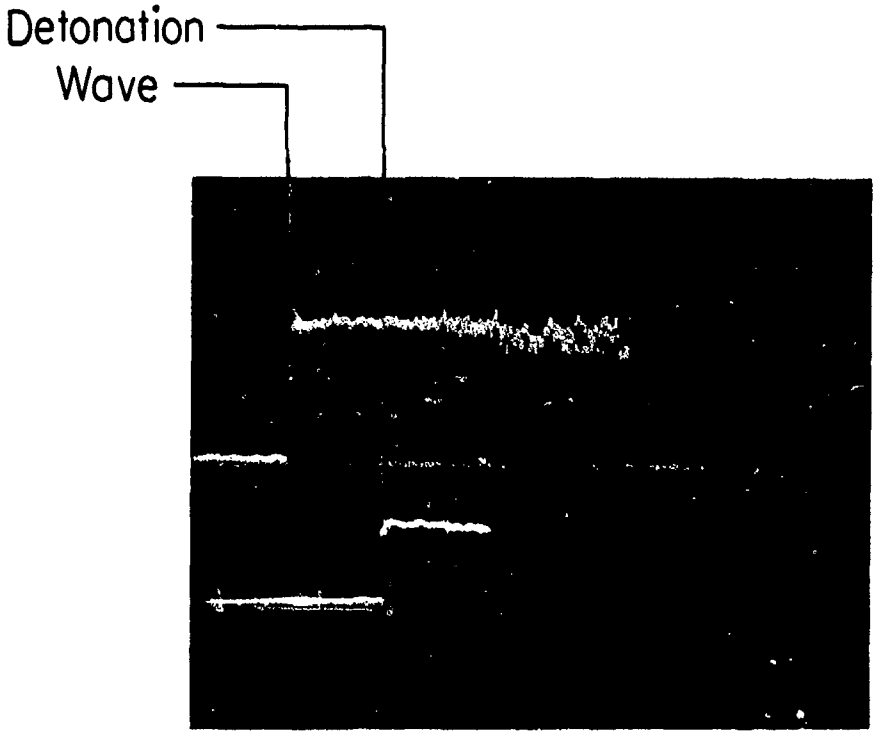

Oscilloscope Setting:

Sweep Rate =0.5 ms/div

Vertical Sensitivity = 20 mV/div

Fig. 9 - A typical oscilloscope trace of a detonation wave traversing a one mole hydrogen-one mole bromine mixture. Driver gas pressure p_4 = 48.72 atm.

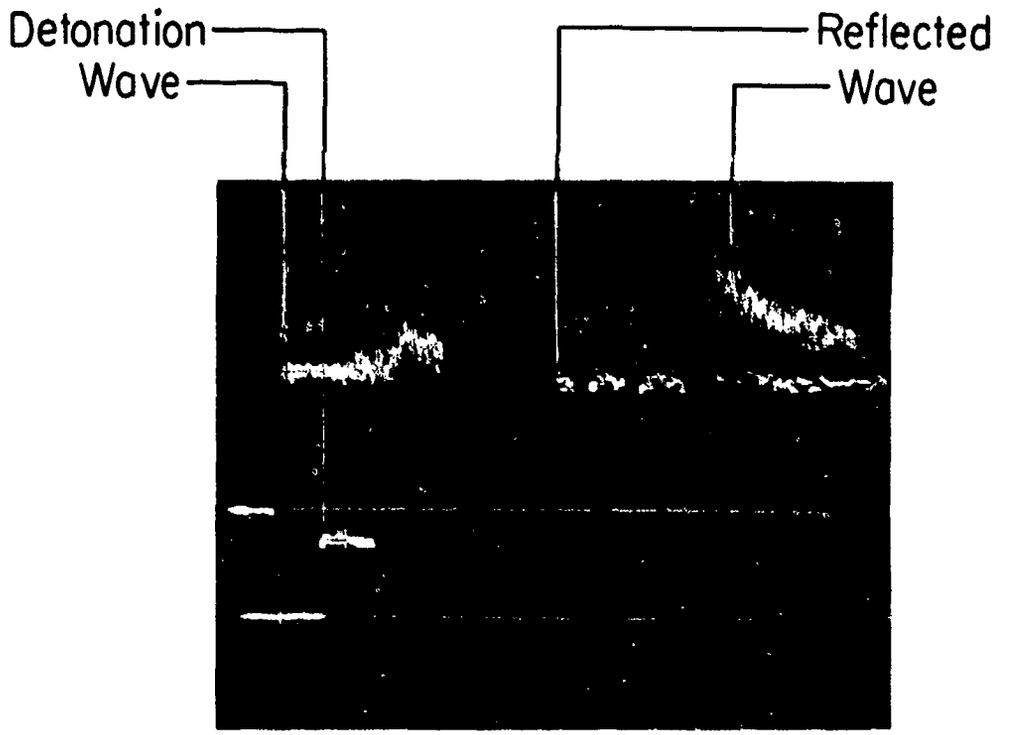

Oscilloscope Setting:

Sweep Rate = 1 ms/div

Vertical Sensitivity = 20 mV/div

Fig. 10 - A typical oscilloscope trace of a detonation wave traversing a one mole hydrogen-one mole bromine mixture. Driver pressure p_4 = 52.80 atm.

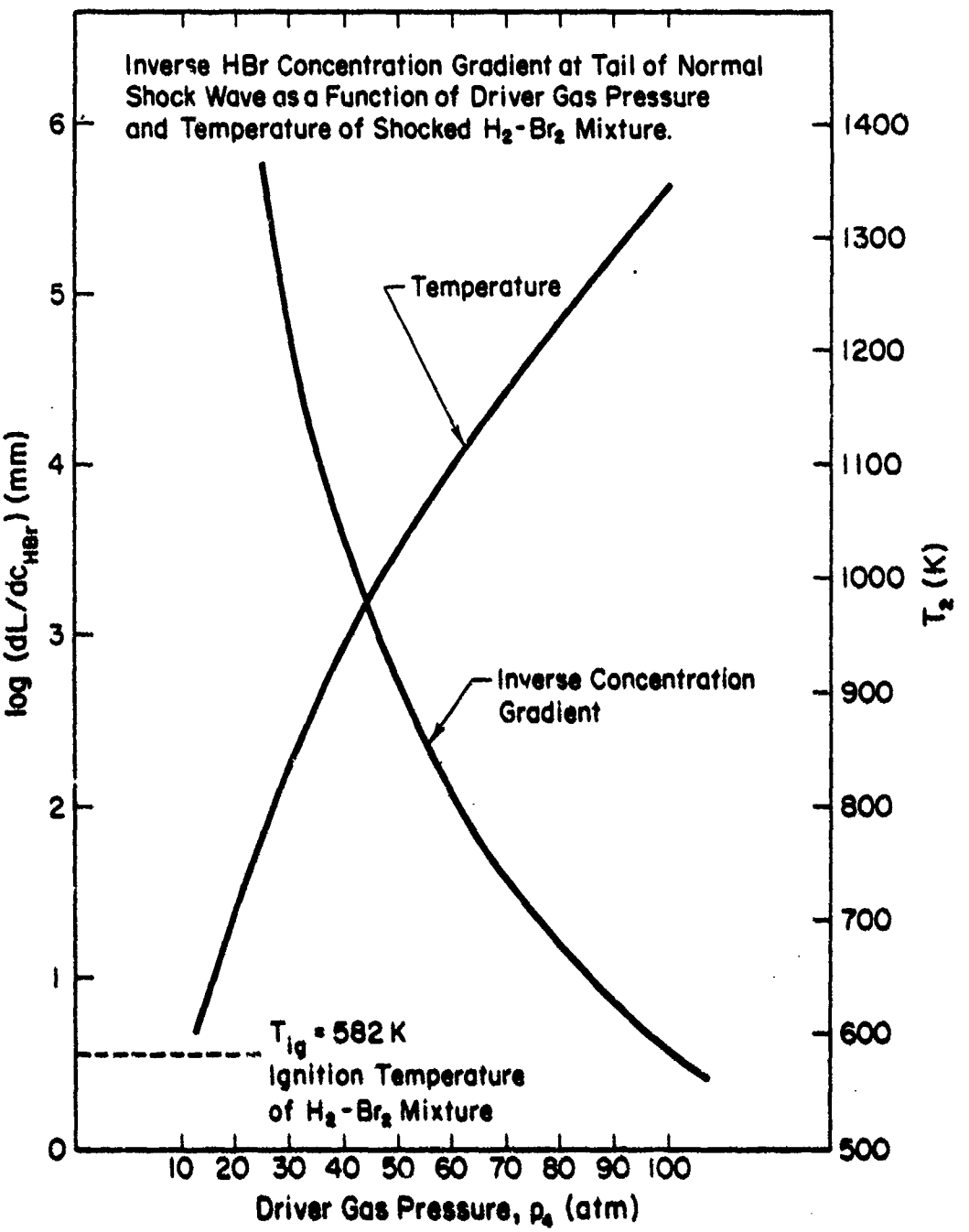

Fig. 11 - Inverse HBr concentration gradient at tail of normal shock wave as a function of driver gas pressure and temperature of shocked H_2-Br_2 mixture

lower than the calculated values (see Fig. 3), indicates that in the shock tube used for these experiments the measured wave speeds are always somewhat lower than the theoretical values.

Although, as shown in Fig. 2, the measured pressures behind shock waves generated in nitrogen agree very well with the theoretical values, a few values observed in hydrogen-bromine mixtures are considerably lower than those calculated for detonation waves. This result appears to indicate that no detonation waves were present in these experiments. However, it was observed that the pressure transducers were extremely erratic after they had been exposed to bromine. Therefore, it was impossible to obtain reliable pressure measurements with the transducers in any gas mixture containing bromine. To obtain reliable pressure measurements in the presence of bromine, it is necessary to develop transducers which are not affected by bromine. Another explanation for the discrepancy between measured and calculated pressure was sought in the use of the thermally perfect gas equation for the calculation of the wave speeds. Unfortunately neither the van der Waals constants, a and b, nor the critical pressure of bromine nor any other equation of state for hydrogen-bromine mixtures are available in the literature. Therefore, it is not possible to calculate the actual pressure behind the waves.

To obtain an approximate insight into the effect of the intermolecular forces on the normal shock wave parameters, calculations of both wave speeds and the pressures behind shock waves passing through carbon dioxide were calculated by including the effect of pressure on enthalpy as obtained by Berthelot's equation of state instead of using pressure independent enthalpies and the equation of state for a thermally perfect gas. The results as shown in Table XVI indicate that for the range of driver gas pressures used the inclusion of intermolecular forces increases the shocked gas pressure by 3% but reduces the wave speeds by less than 2%. According to these results the observed discrepancies cannot be attributed to the real gas behavior of the hydrogen-bromine mixture.

However, support for the observation that stable detonation waves are produced in hydrogen-bromine mixtures comes from the calculation of the reaction zone length on the basis of the simple nonbranching chain mechanism. As shown in Figs. 5-7 the arbitrarily selected ratio of the hydrogen bromide mole fraction to that of atomic bromine or atomic hydrogen (Profiles 1 and 2) has practically no influence on the thickness of the reaction zone and it modifies the shapes of the pressure and temperature profiles in the reaction zone (Fig. 7) only slightly. Most significant is the fact that the formation of HBr is more than 93% complete at a distance of slightly less than 0.15 mm downstream of the tail of the normal shock wave and that the length required to establish complete equilibrium is only 0.75 mm. Even this length does not seem to be too long and must be considered to be quite compatible with the existence of a stable detonation wave in the 1 mole hydrogen - 1 mole bromine mixture.

Table XVI. Effect of intermolecular forces on shock wave parameters in carbon dioxide (T_c = 304.25 K, p_c = 73 atm); (T_1 = 200 K p_1 = 1 atm)

p_4 (atm)	T_2 (K)	p_2 (atm)	ρ_2 (kg/m^3)	w_1 (m/s)	u_2 (m/s)	$z = \frac{p_2 v_2}{\Re T_2}$
20	410	8.60	11.30	614	469	1.0000*
	415	8.85	11.84	605	462	0.9660**
30	465	11.03	12.85	697	551	1.0000*
	469	11.28	13.42	687	543	0.9612**
40	506	13.03	13.90	756	612	1.0000*
	510	13.30	14.56	747	601	0.9606**
50	543	14.92	14.74	803	659	1.0000*
	546	15.23	15.42	791	648	0.9702**
60	574	16.51	15.41	841	696	1.0000*
	576	16.90	16.11	819	686	0.9769**

*Thermally perfect equation of state.

**Berthelot equation of state.

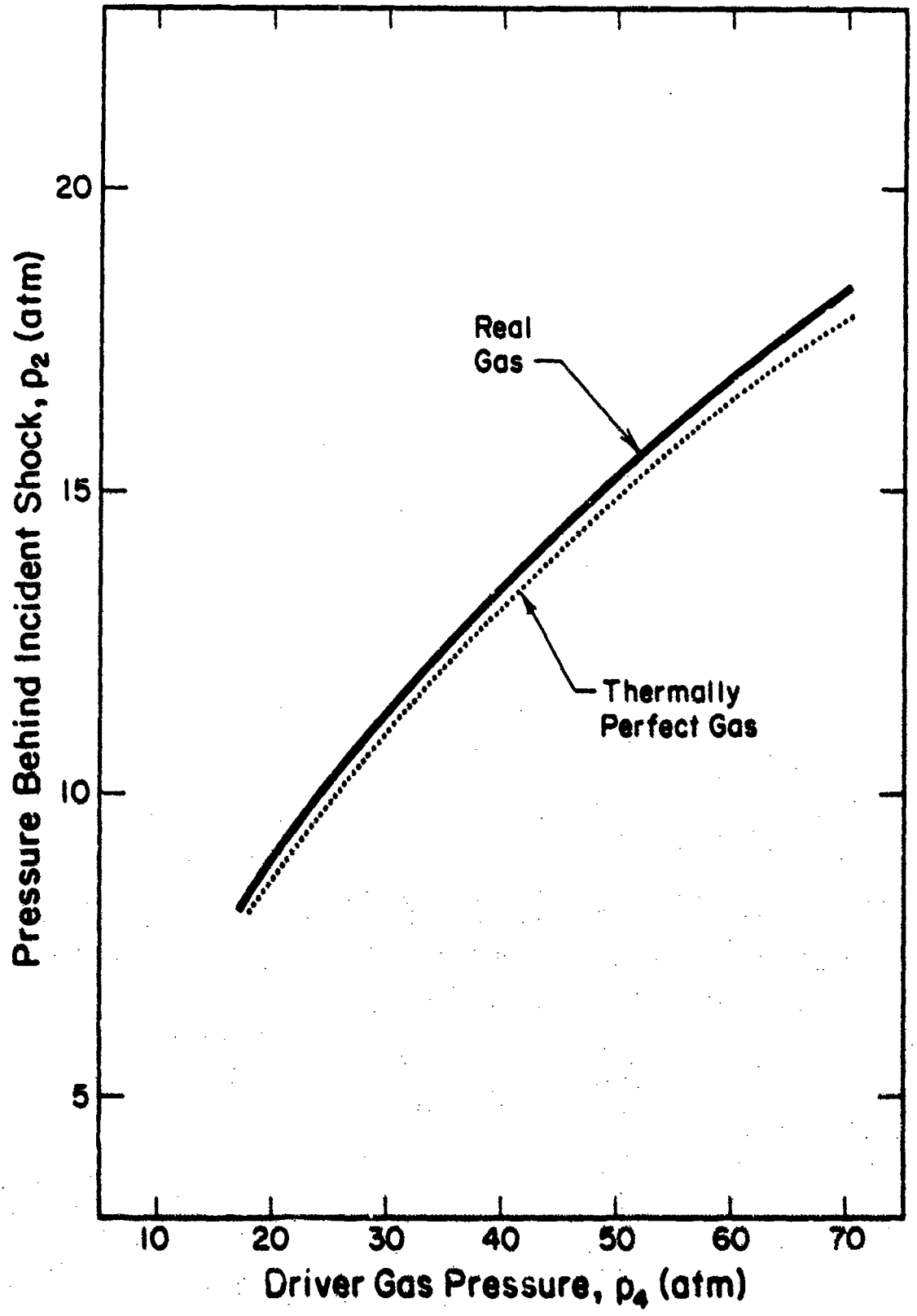

Fig. 12 - Pressure, p_2, behind an incident normal shock wave in CO_2 (p_1 = 1 atm, T_1 = 200 K) as a function of driver gas (helium at 300 K) pressure, p_4

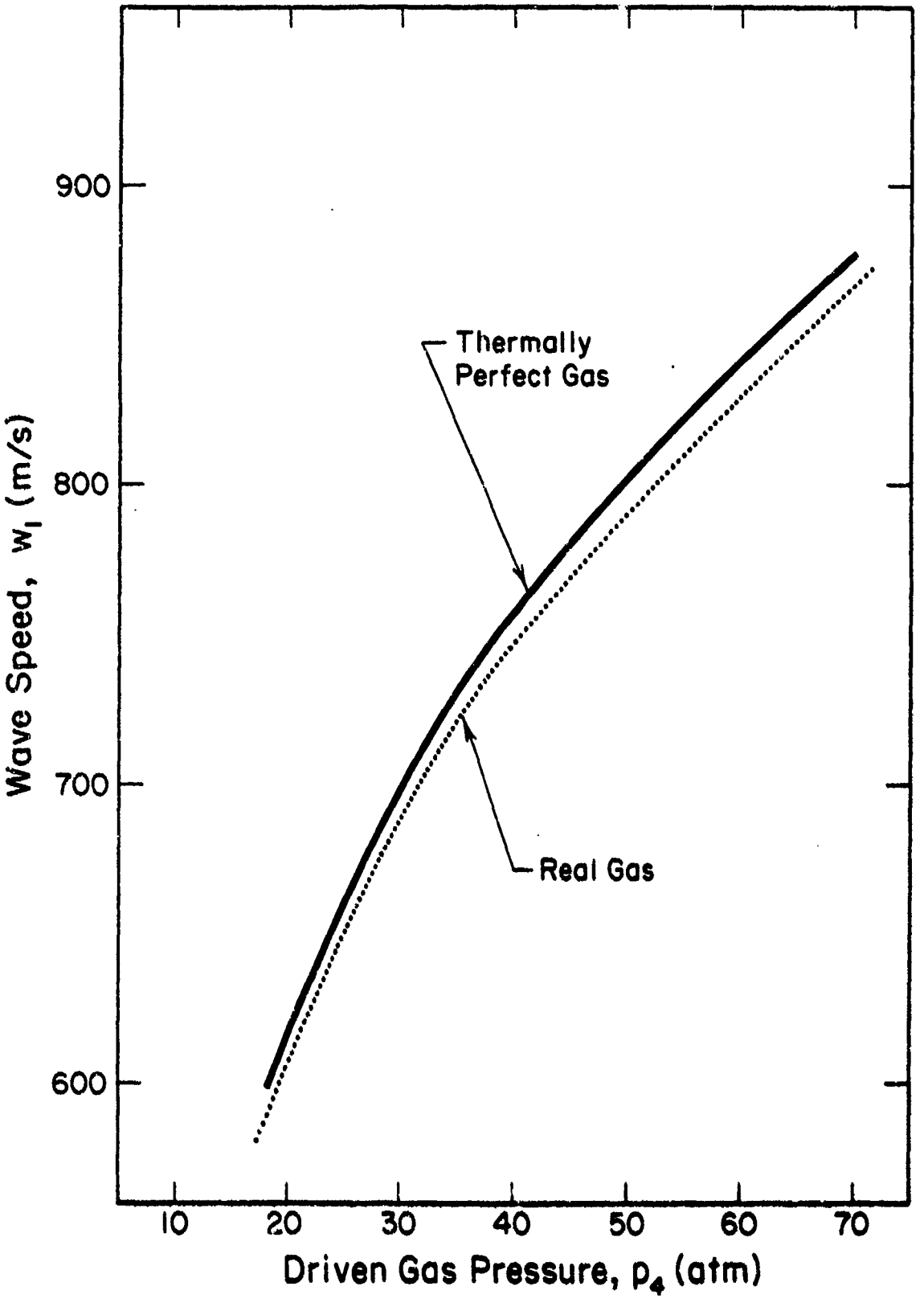

Fig. 13 - Wave speed, w_1, of an incident normal shock wave in CO_2 ($p = 1$ atm, $T_1 = 200$ K) as a function of driver gas (helium at 300 K) pressure, p_4

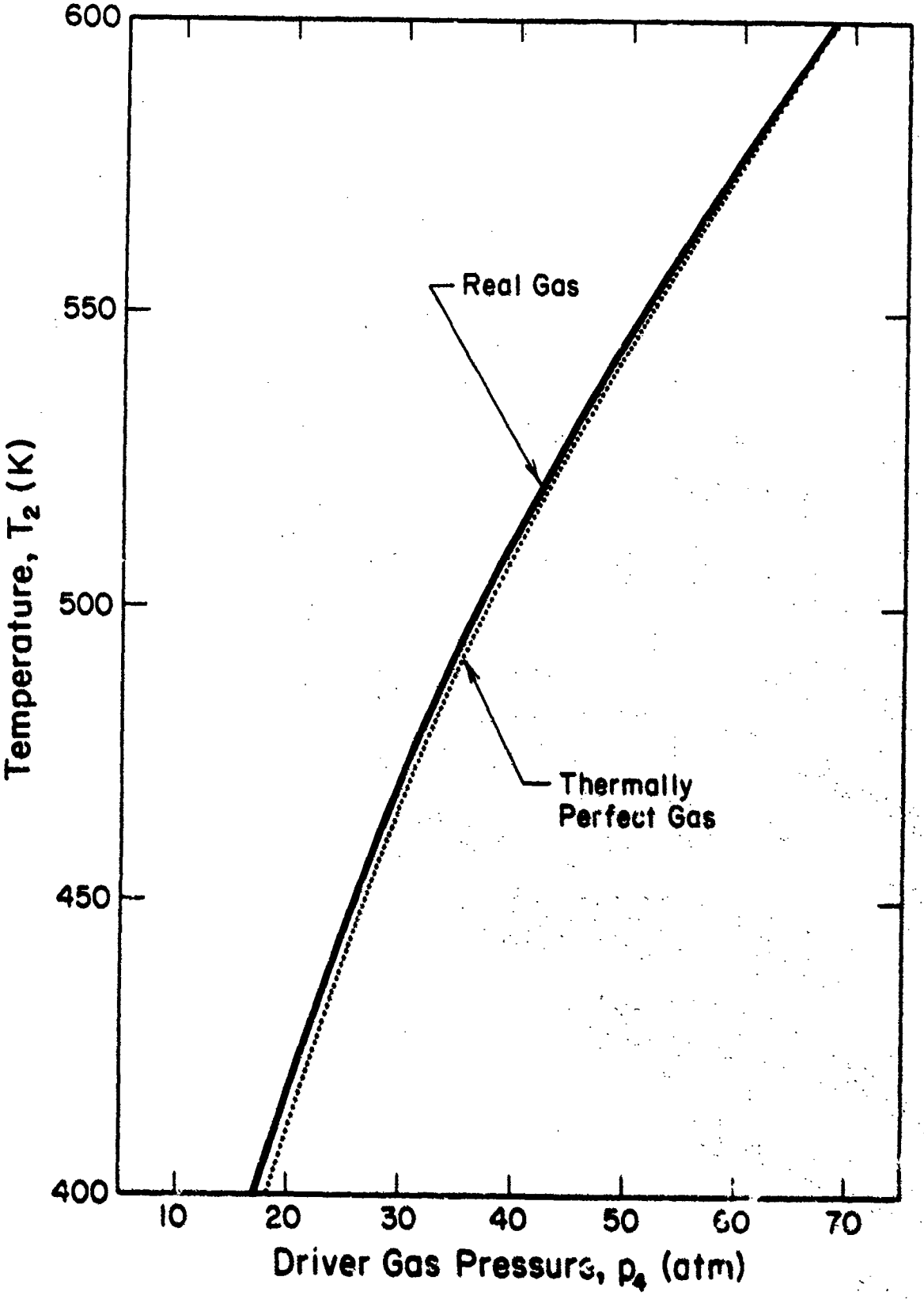

Fig. 14 - Temperature, T_2, behind an incident normal shock wave in CO_2 (p_1 = 1 atm, T_1 = 200 K) as a function of driver gas (helium at 300 K) pressure, p_4

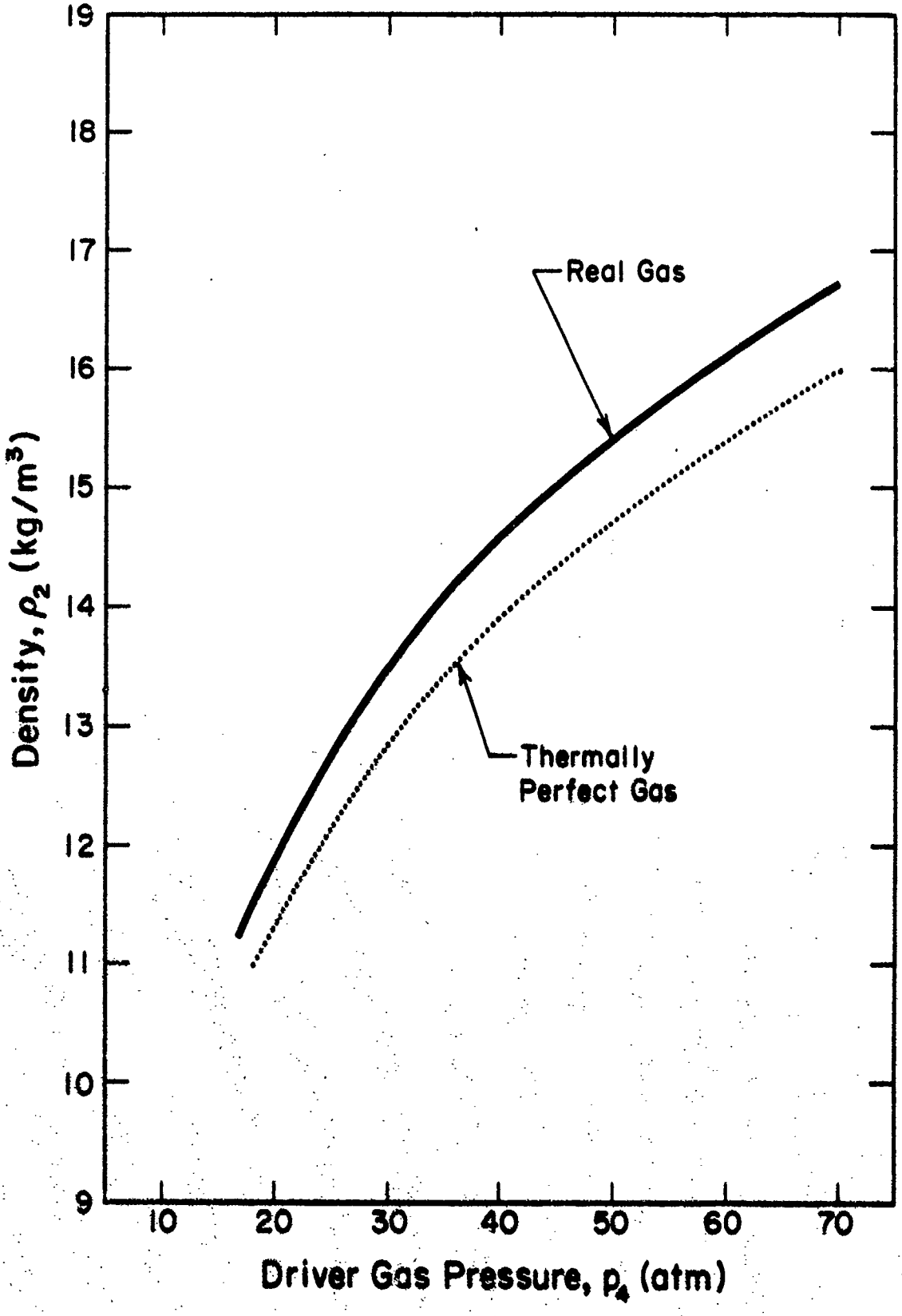

Fig. 15 - Density, ρ_2, behind an incident normal shock wave in CO_2 (p_1 = 1 atm, T_1 = 200 K) as a function of driver gas (helium at 300 K) pressure, p_4

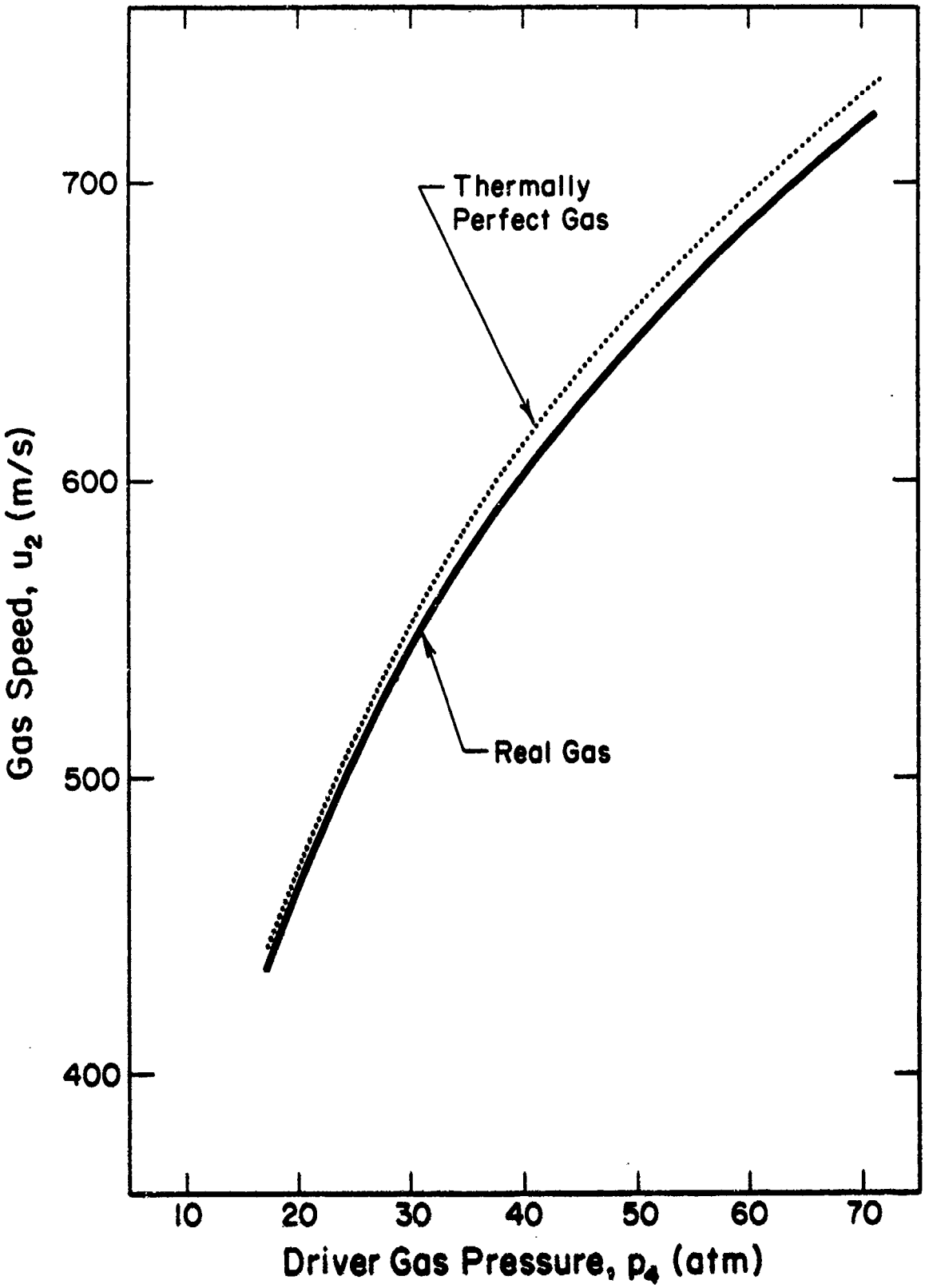

Fig. 16 - Speed of gas, u_2, behind an incident normal shock wave in CO_2 (p_1 = 1 atm, T_1 = 200 K) as a function of driver gas (helium at 300 K) pressure, p_4

II. FLAME QUENCHING

Experiments to study the mechanism of flame quenching of gaseous fuel-oxidizer mixtures by means of plastic and metallic foams were started in September, 1976. Schematic views of the apparatus used for these experiments are shown in Figs. 17 and 18. Four different foams, as supplied by the Air Force Aero-Propulsion Laboratory at Wright-Patterson Air Force Base, were used; i.e., (1) a blue polyester with 10 pores per inch, (2) a red polyester with 20 pores per inch, (3) an orange polyester with 10 pores per inch, and (4) an Explosafe aluminum sponge with 10 pores per inch.

From an extensive test program with methane-air flames and the four materials listed above, the following results were obtained:

(1) When equal thicknesses of the quenching foams were used, aluminum is by far the most effective quenching material.

(2) Polyester foam with 20 pores per inch is more effective than the identical material with 10 pores per inch. To be as effective in quenching methane-air flames as the 20 pores per inch material, much thicker layers of the 10 pores per inch polyester had to be used.

(3) Temperature measurements made with Chromel-Alumel thermocouples both upstream and downstream of the test section indicate that for a completely quenched flame the temperature of the gases just downstream of the test section is decreased to room temperature. In this case no re-ignition of the downstream reactant gas mixture takes place. However, for a partially quenched flame re-ignition always occurred downstream of the arrestor although the flame gases were not luminous after they had passed through the quenching material. This absence of radiation, as observed visually, was confirmed later by high-speed photographs, shown in Fig. 19. The gas temperature of the partially quenched flame gases was of the order of 700 K.

(4) Pressure measurements made with Kistler Quartz pressure transducers both upstream and downstream of the test section always showed a moderate decrease in pressure across the arrestor.

(5) Flame speed measurements made with Texas Instruments LS 400 photo diodes indicate that for higher flame speeds thicker layers of foam are needed to produce complete quenching of the flame.

After several series of experiments had been completed in this apparatus it became obvious that this technique was not producing quantitative results. An investigation of flame quenching by means of foams has the following shortcomings:

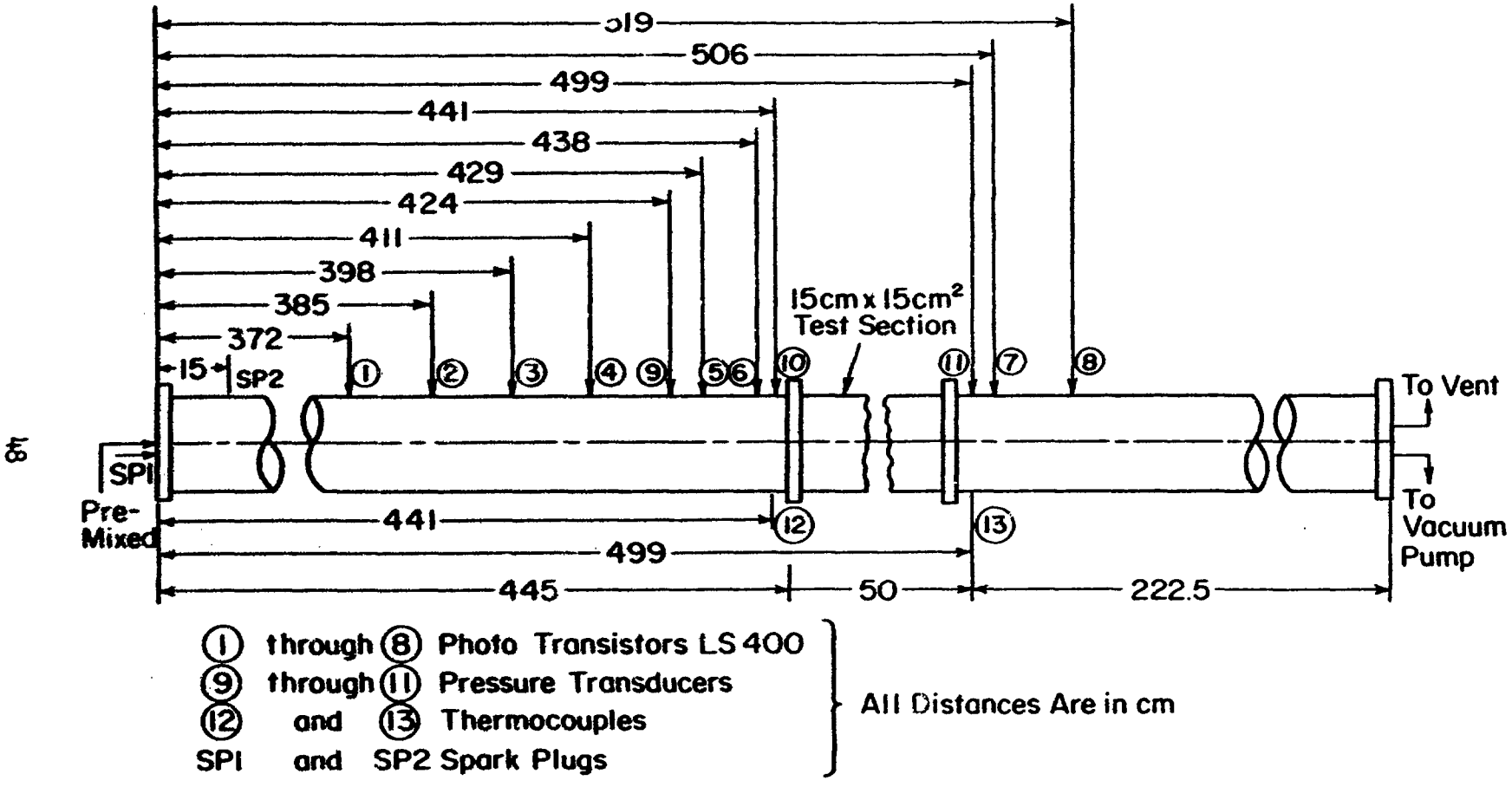

Fig. 17 - Schematic view of the 15 cm I.D. combustion tube for flame quenching studies

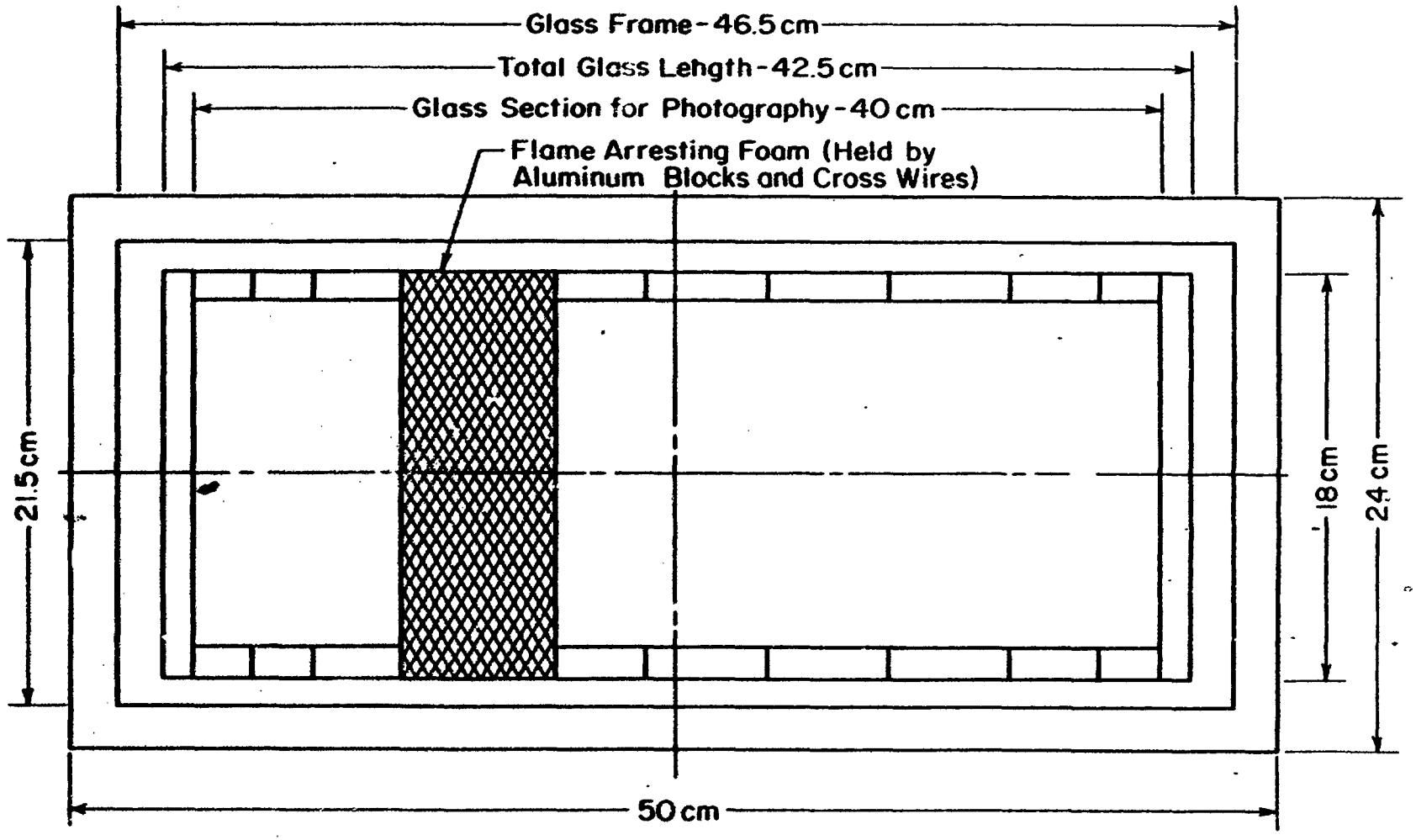

Fig. 18 - Test section detail (scale 1/2 full size) of flame arrestor

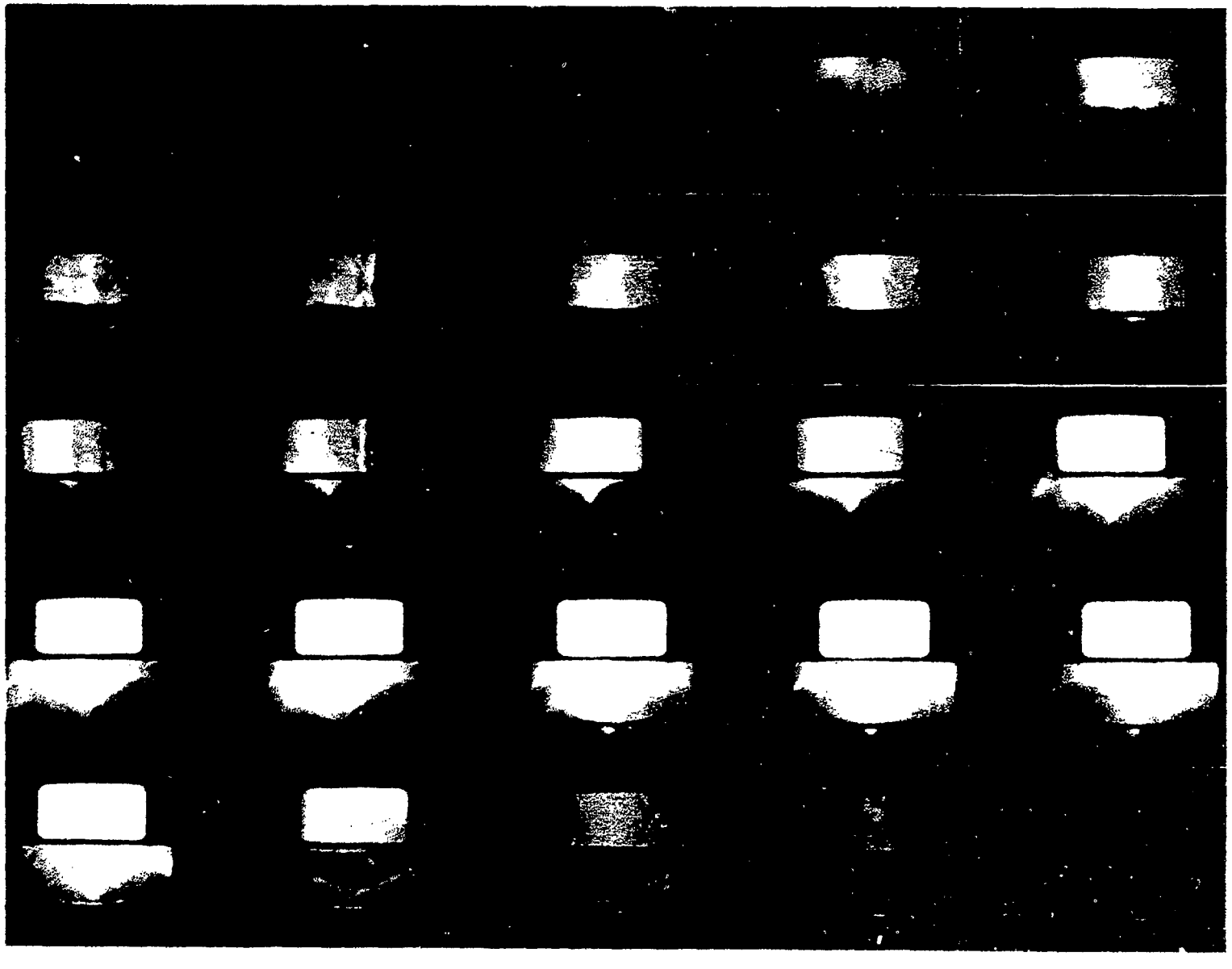

Fig. 19 - High speed photograph (6000 fps) of quenched CH_4-air flame (u_f = 40 m/s)

It does not afford an insight into the mechanism of flame quenching. For instance, to determine the role of heat transfer in flame quenching it is necessary to know the thermal conductivity of the foam material which is not available for these foams. To understand the role played by destruction or activation of radicals at the foam surface, optical spectroscopy or mass spectrometry must be employed, both of which cannot be used with foams. Several experiments were made to obtain some spectroscopic record during the quenching process. Whereas a spectrogram of the flame just upstream of the arrestor can be obtained quite readily, it is impossible to obtain any record inside the foams because the foams decompose and form all kinds of products. Furthermore, the luminosity of the flame is reduced to such a low value that it becomes necessary to employ either absorption spectroscopy or to use a high-speed prism spectrograph with low resolving power. Mass spectrometry also cannot be employed very well because of the transient nature of the process.

Since the principal objective of the flame quenching study is to understand the mechanism of flame quenching so that an effective arrestor can be designed without the need of an extensive test program, another approach was explored.

To obtain direct visibility of the quenching process for spectroscopic studies and for a simple observation of the effect of wall material on the fate of active centers or radicals, a 33 cm pyrex glass tube, divided into three sections, was designed and constructed. The first section of the tube was 15 cm long and had an I.D. of 10 mm; the second section consisted of an 8 cm-long, 2 mm-I.D. pyrex glass capillary; and the third section was again a 10 cm pyrex glass tube having an inner diameter of 10 mm. The tube was filled with a fuel-oxidizer mixture which was ignited with a spark at one end of the vertically mounted tube. In principle this arrangement made it possible to follow the quenching process of the flame along the entire length of the tube and to obtain photographic and spectroscopic records.

Since the amount of heat transferred from the flame to the glass is very small, this set-up permits a good study of the role of diffusion and subsequent destruction of various radicals at the walls of the arrestor.

Also, flowing gases can be analyzed in this manner. Finally, the contribution of the effect of buoyancy on flame quenching can be ascertained by igniting the gas mixture either at the top or the bottom end of the vertically mounted tube. After a brief series of experiments, however, it became apparent rather quickly that most of the expectations were not fulfilled.

Although the 2 mm capillary was quite effective in quenching methane-air flames, the light emitted by the flame was too weak to produce a spectroscopic record even with a high-speed prism spectrograph. To obtain a more luminous process a methane-oxygen flame was tried. Although no detonation occurred, the glass tube broke into many pieces. Apparently the capillary offered too much resistance to the rapidly propagating flame

and the resulting over-pressure, together with the thermal stress, caused the tube to disintegrate.

Because of these difficulties it was decided to design an apparatus which would make the quenching process stationary. To accomplish this objective a rectangular burner with a high length-to-width ratio was constructed. On each long side of the burner is a planar movable block of some specially selected material. Both quenching blocks can be moved symmetrically to squeeze in on the flame until it is quenched [see Figs. 20(a), 20(b), and 21]. In this manner any phase of the quenching process can be maintained for indefinite periods so that long exposure times for spectroscopic photographs become available. Two different size burner tubes were used; i.e., burner No. 1 [see Fig. 20(a)] with a length-to-width ratio of $\frac{L}{w} = \frac{0.64 \text{ cm}}{0.16 \text{ cm}} = 4$; and burner No. 2 [see Fig. 20(b)] with $\frac{L}{w} = \frac{2.50 \text{ cm}}{0.32 \text{ cm}} = 7.8$, in order to obtain laminar flames with fast and slow flames. The different ratios also permit an assessment of the effect of the unquenched short sides of the rectangular flame on the observed quenching distances.

For the first series of experiments the quenching blocks were made of solid copper with internal channels for water cooling. A copper-constantan thermocouple was embedded in each block for measuring their surface temperatures. Two copper-constantan thermocouples were also used (a pair for each block) to measure the temperature of the water entering and leaving the blocks. The output of these six thermocouples was recorded on a 14-channel Honeywell type recorder. In all experiments the blocks were maintained at a constant temperature by proper adjustment of the flow of water. The two copper blocks were bolted to two metal platforms which could be moved inward and outward with the help of a hand-operated spindle. The two blocks were mounted in such a fashion that they rested on the burner rim when they approached the burner tube and then could be moved over the burner rim until quenching of the flame was complete. The quenching distances were measured with a feeler gauge which had an accuracy of 0.001 cm. The entire assembly (i.e., blocks, spindle, etc.) was in turn bolted to the optical bar of a 21-foot grating spectrograph. A rectangular opening in the center of the optical bar allowed the burner to be placed in the center between the two blocks and made it possible to focus the flame on the slit of the spectrograph. The burner assembly could also be mounted on the optical bar of a Hilger & Watts prism spectrograph for qualitative work with moderate resolution. A photograph of the burner and quenching blocks is shown in Fig. 21.

With this design of the apparatus for the study of flame quenching, the following aspects of the quenching process have been studied:

(1) The variation of species concentration and flame temperature as quenching progresses by means of spectroscopic measurements.

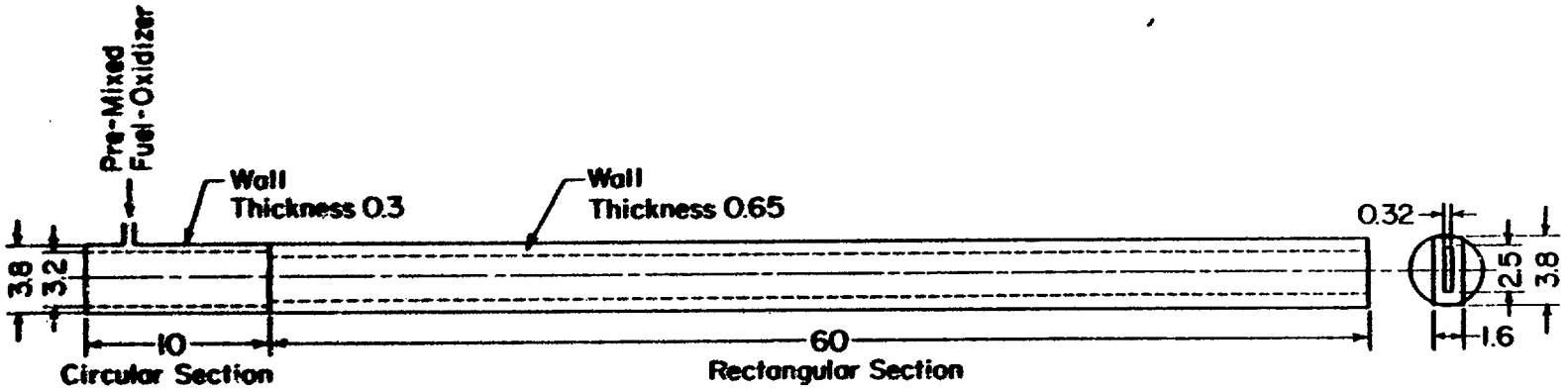

Fig. 20(a) - Rectangular burner No. 1 for flame quenching experiments

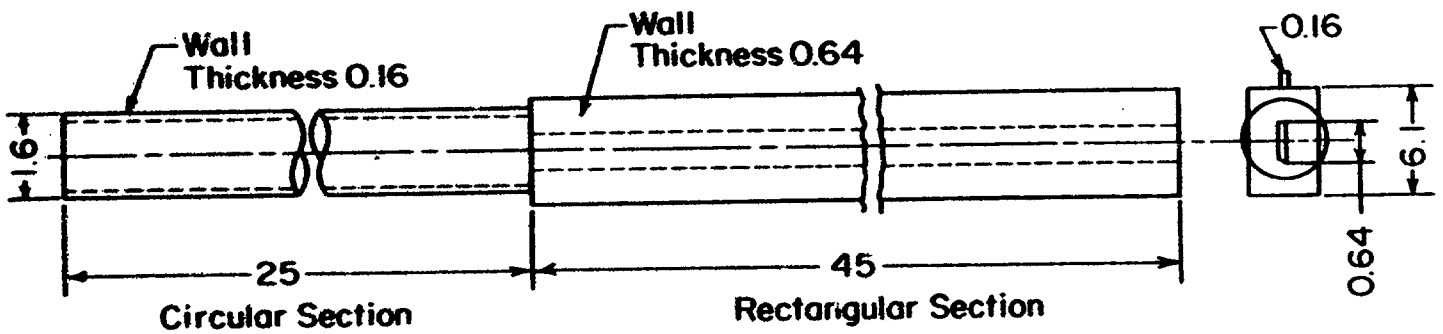

Fig. 20(b) - Rectangular burner No. 2 for flame quenching experiments

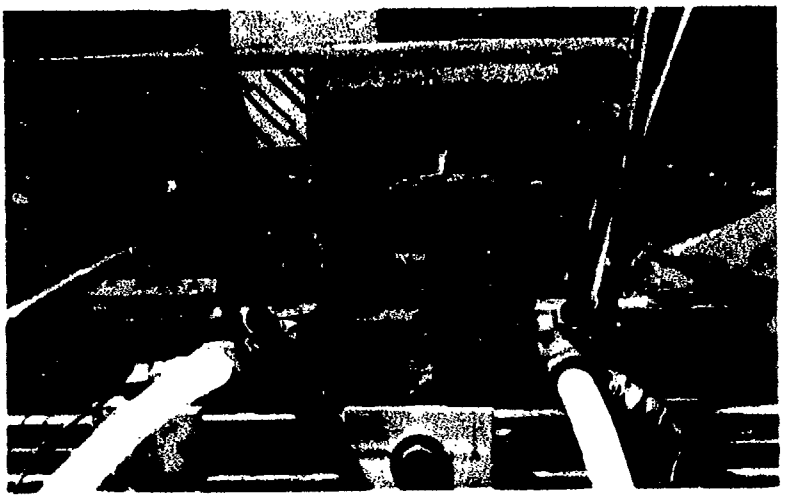

Fig. 21 - Photograph of rectangular burner with movable quenching blocks

(2) The contribution of heat transfer to quenching effectiveness by using different materials for the quenching blocks.

(3) The behavior of different fuel-oxidizer mixtures.

(4) The effects of flame speed, flame temperature, linear speed of the unburned gas, and Reynolds number on the quenching distance.

(5) The role of surface catalysis on flame quenching by using different materials for the quenching blocks or by applying special surface coatings.

(6) The effect of initial temperature of the quenching blocks on the quenching distance.

(7) The analysis of the flame gas by collecting samples of the burned gas.

It is intended to use the experimental results for the development of a theory of flame quenching which will enable the designer of flame arrestors to produce a device which is most effective for the particular problem on hand.

Experimental measurements carried out so far have yielded the following results:

(1) The quenching distances of methane-air flames are greatly increased when the quenching blocks are coated with chloro-bromomethane. However, copper blocks produce only slightly larger quenching distances than blocks of mica (see Fig. 22).

(2) The quenching distances of methane-oxygen flames are much smaller than those of methane-air flames; they exhibit the same behavior toward surface coatings and materials (see Fig. 23).

(3) The quenching distances of hydrogen-air flames are only slightly larger than those of methane-oxygen flames. However, the influence of surface coating and material is similar to that on methane-fuel flames (see Fig. 24).

(4) In spite of the lower flame speeds of acetylene-air flames, their quenching distances were found to be quite similar to those of hydrogen-air flames at all conditions investigated (see Fig. 25).

(5) The effect of adding inert gases to the combustible gas mixture has been investigated for hydrogen-oxygen flames. The results are shown in Figs. 26 and 27. As to be expected, the quenching distances increase with increasing inert gas concentration. However, there is hardly any difference in effect between argon, nitrogen, and carbon dioxide in the vicinity of the maximum

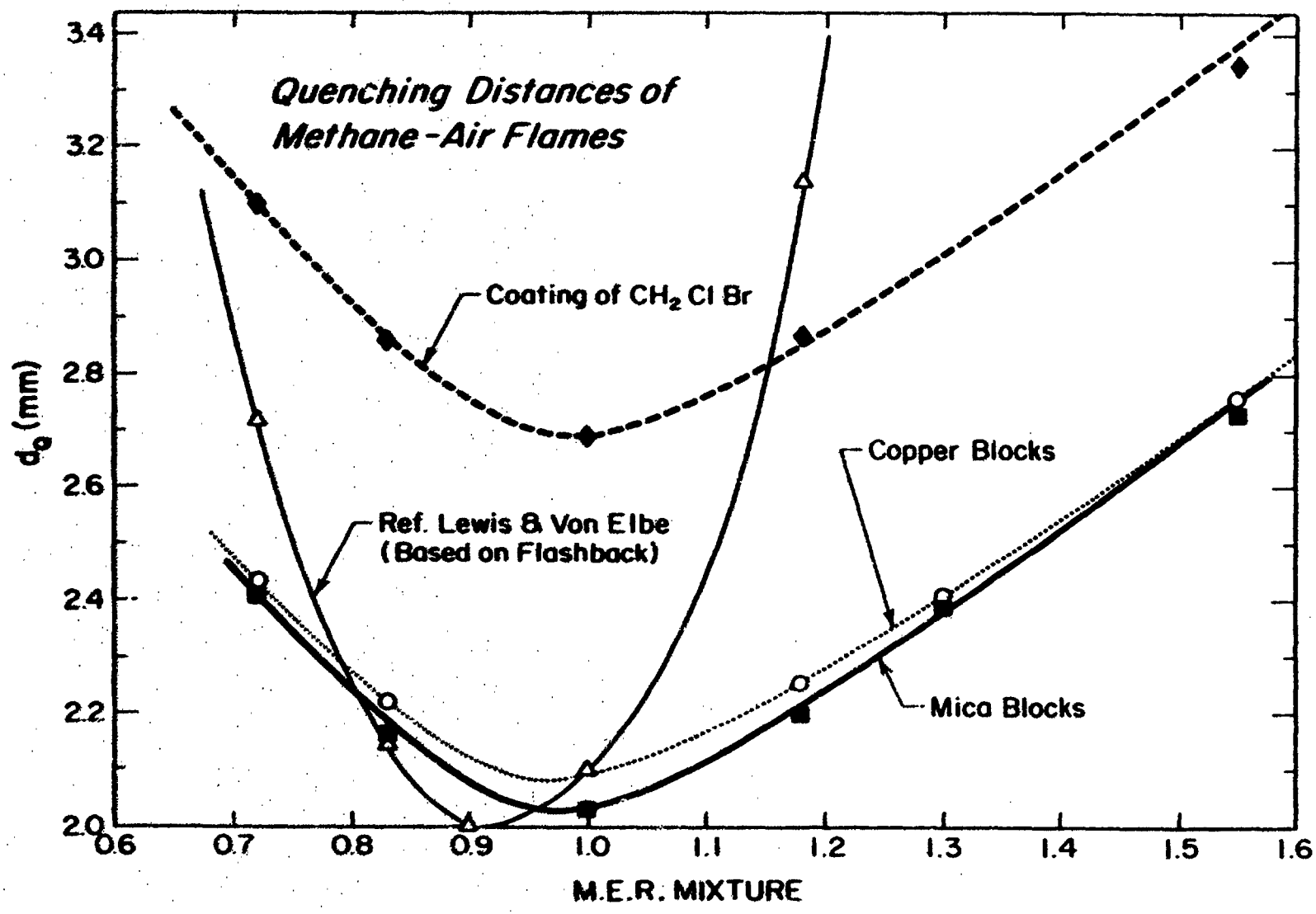

Fig. 22 - Quenching distances of methane-air flames

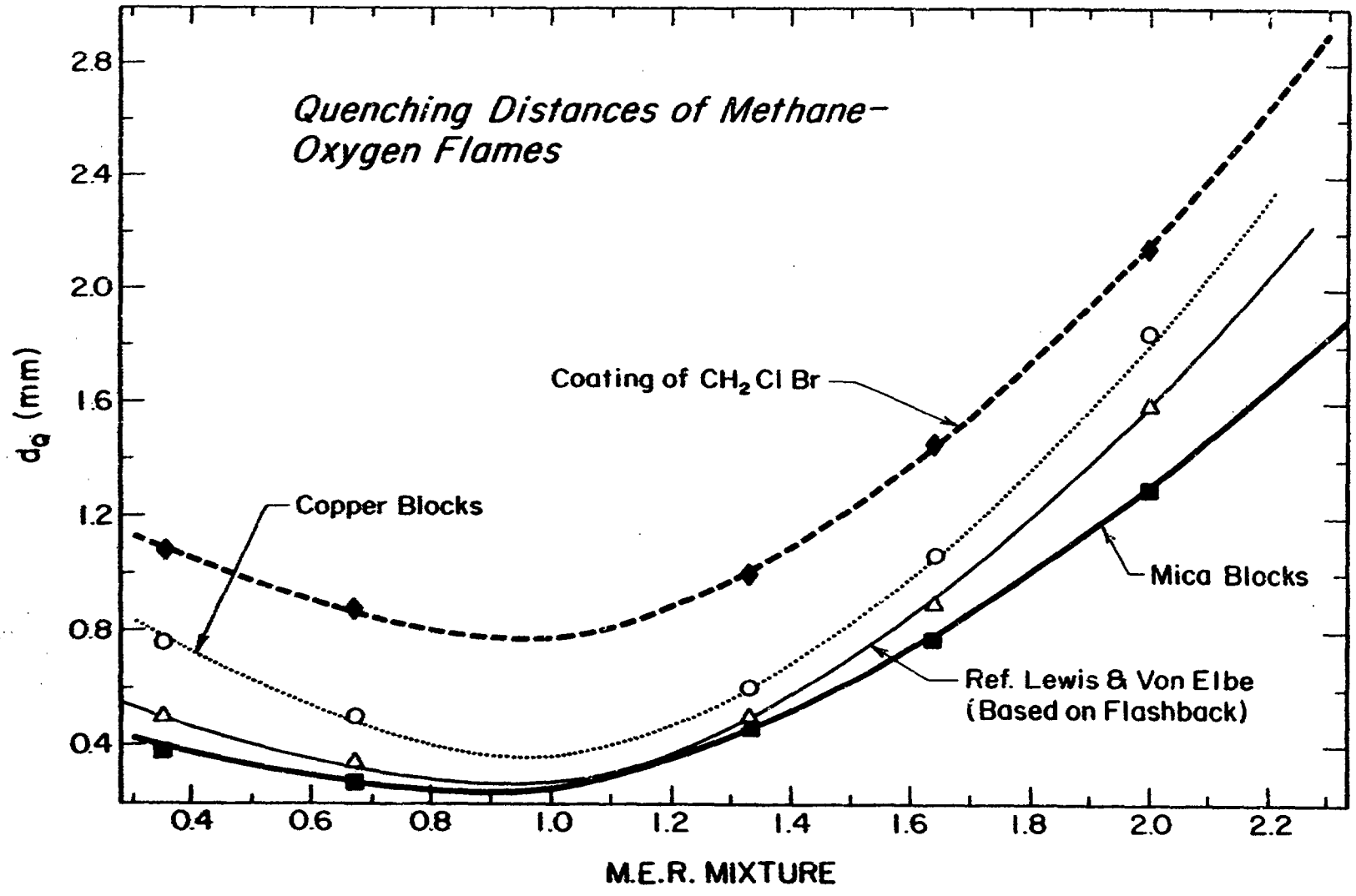

Fig. 23 - Quenching distances of methane-oxygen flames

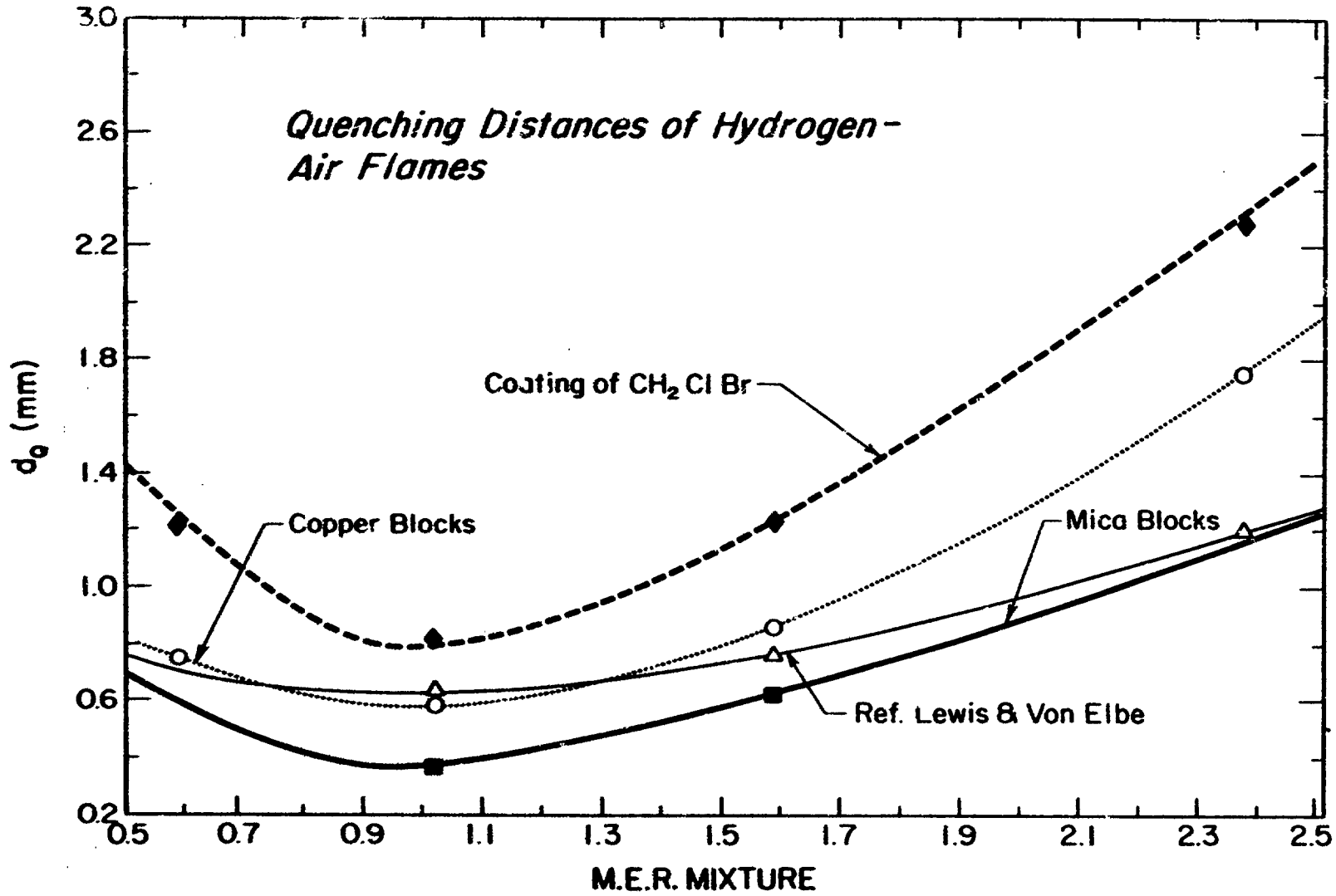

Fig. 24 - Quenching distances of hydrogen-air flames

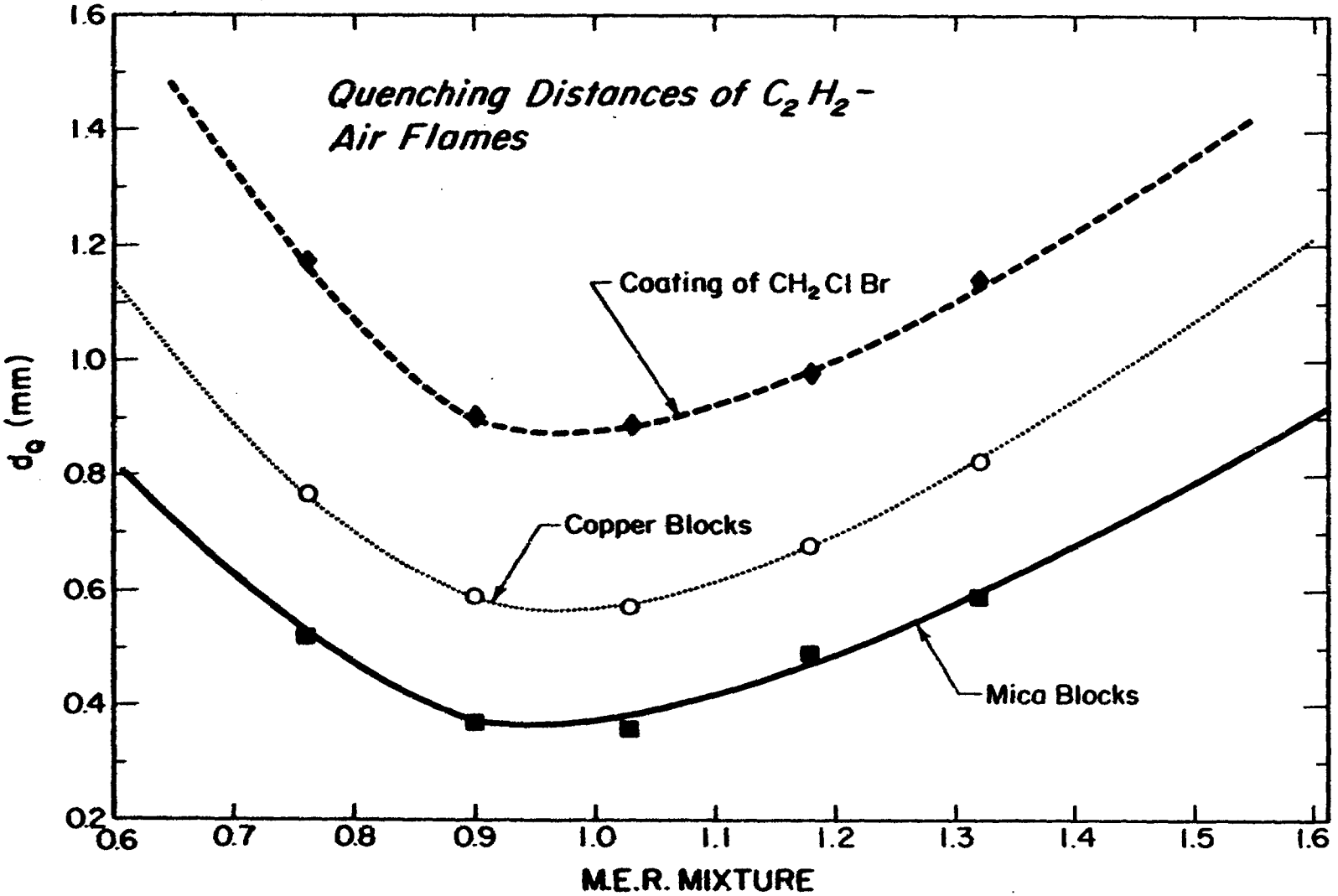

Fig. 25 - Quenching distances of C_2H_2-air flames

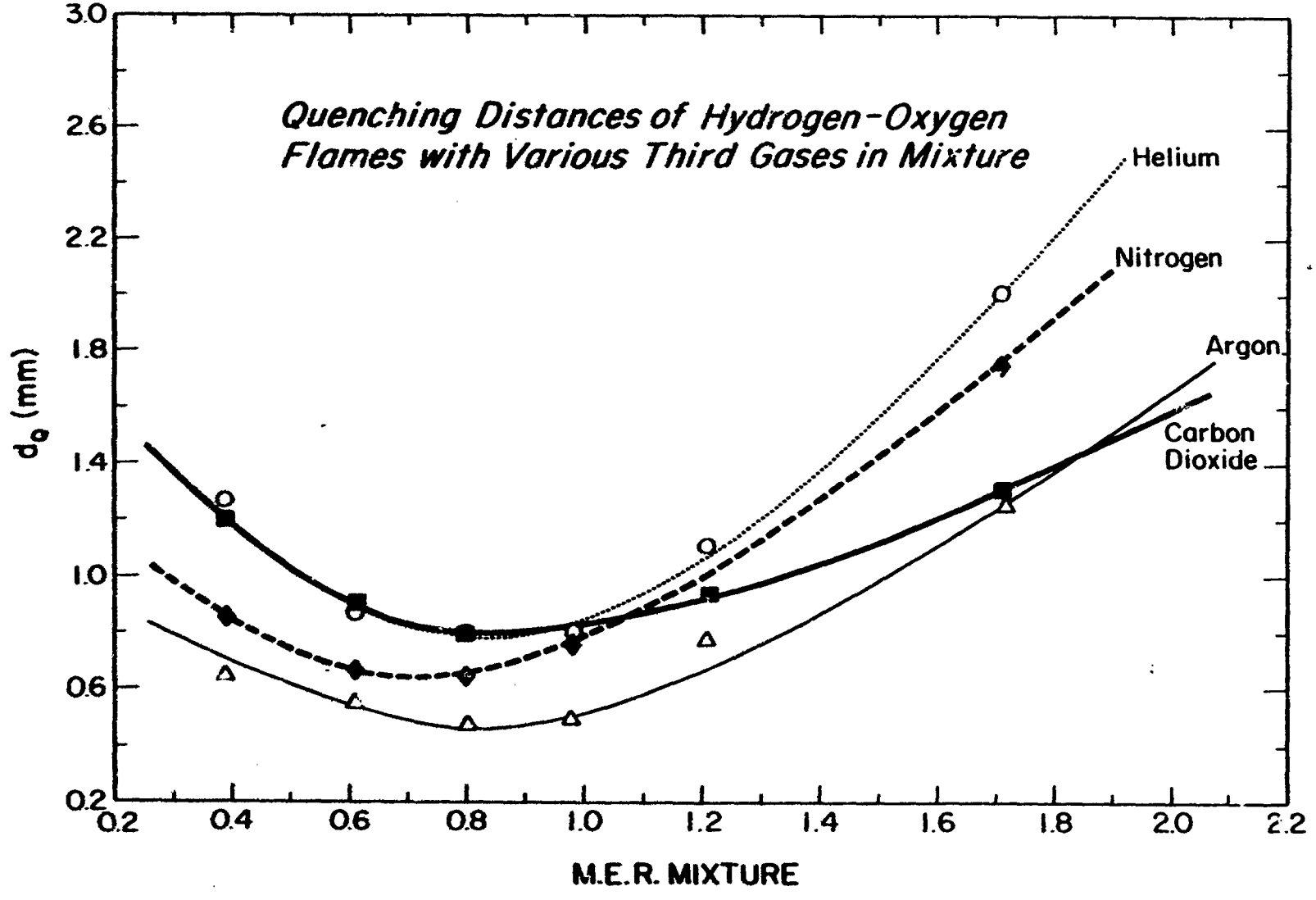

Fig. 26 - Quenching distances of hydrogen-oxygen flames with various third-gases in mixture

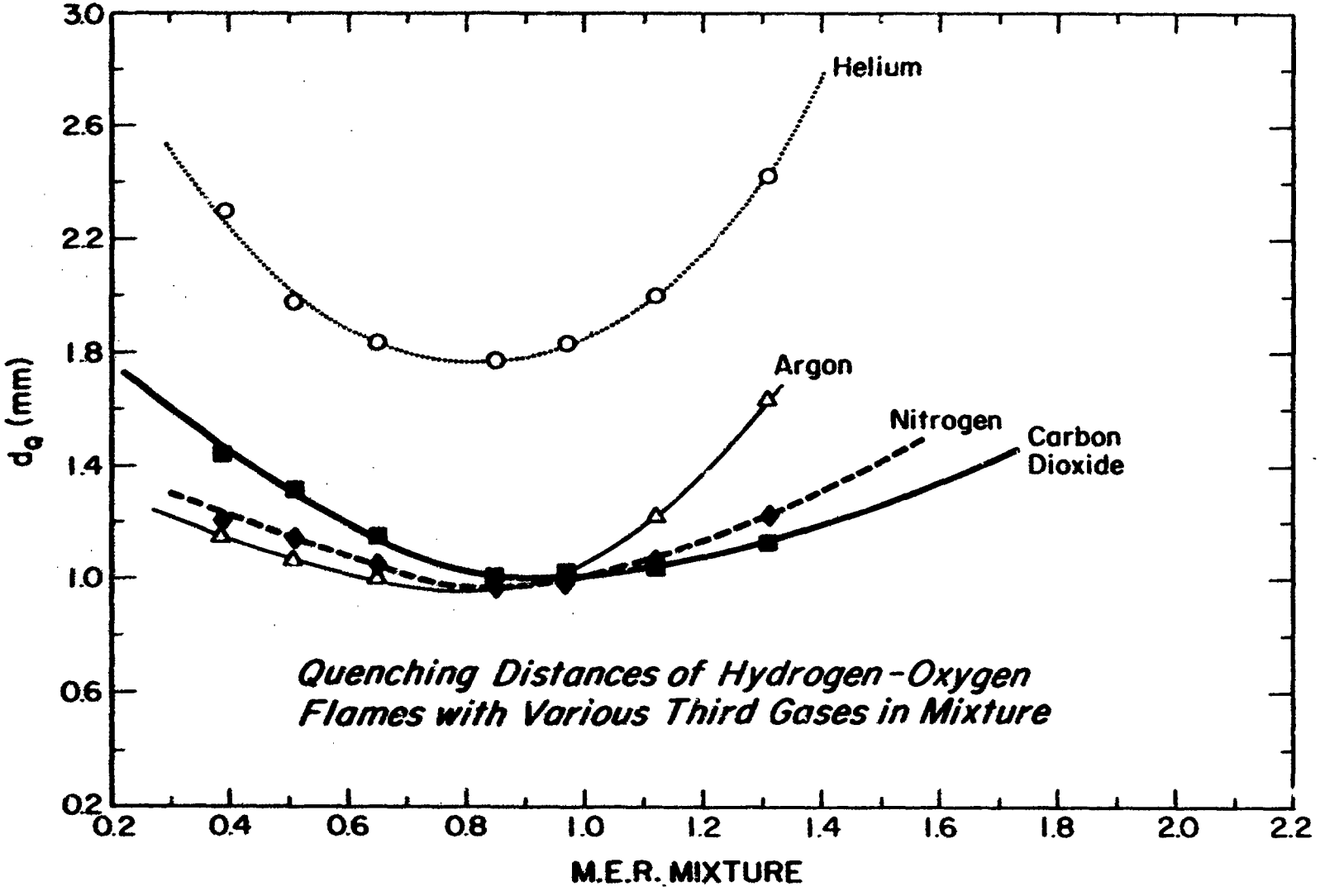

Fig. 27 - Quenching distances of hydrogen-oxygen flames with various third-gases in mixture

energy composition, whereas helium addition produces a rather significant increase of the quenching distance. Since helium is much more effective than argon it is obvious that the high thermal conductivity of helium is responsible for the large increase in the quenching distance. In fuel-rich flames nitrogen produces a greater increase in the quenching distance than argon, whereas the reverse is true for lean flames. Also helium and nitrogen produce the same quenching distance in lean mixtures having 55.6% inert gas. More experiments are needed to understand the reason for these apparent contradictions. At this point, there seems to be no simple correlation between any of the properties of the various gases and the effect on the quenching. The only outstanding feature is the high thermal conductivity of helium which is only slightly less than that of hydrogen, whereas the conductivities of the other gases are an order of magnitude smaller; carbon dioxide has by far the lowest conductivity. On the other hand, the flame temperature of a hydrogen-oxygen-helium (or argon) mixture is almost 500 K higher than that of a mixture in which the helium is replaced by carbon dioxide. Also the flame speed of the mixture containing helium is considerably higher than that of the mixtures containing N_2, A, or CO_2 (see Figs. 28 and 29).

(6) Several spectrograms of methane-air flames at various stages of the quenching process revealed a significant change in the composition and temperature of the combustion gas. However, measurements of the rotational intensity distributions showed that the distribution of energy in the rotational mode is not in equilibrium. The observed rotational temperatures of the partially quenched flames were unrealistically high; e.g., 6000 to 11000 K (see Figs. 30 and 31). Measurements made with thermocouples indicated that the temperatures of partially quenched flames are actually much lower than the normal flame temperatures.

In general it can be concluded from the experimental study carried out so far that:

(1) For a given combustible gas mixture the quenching distance is independent of the shape of the burner, the linear gas speed in the burner tube, and the Reynolds number of the unburned gas flow.

(2) The quenching distance is dependent on flame speed, flame temperature, fuel-to-oxidizer mass ratio, type and nature of quenching surface, and thermal conductivity of burned gas.

(3) The effectiveness of surface coatings varies greatly from one material to another. It appears that substances which are good chain breakers are most effective.

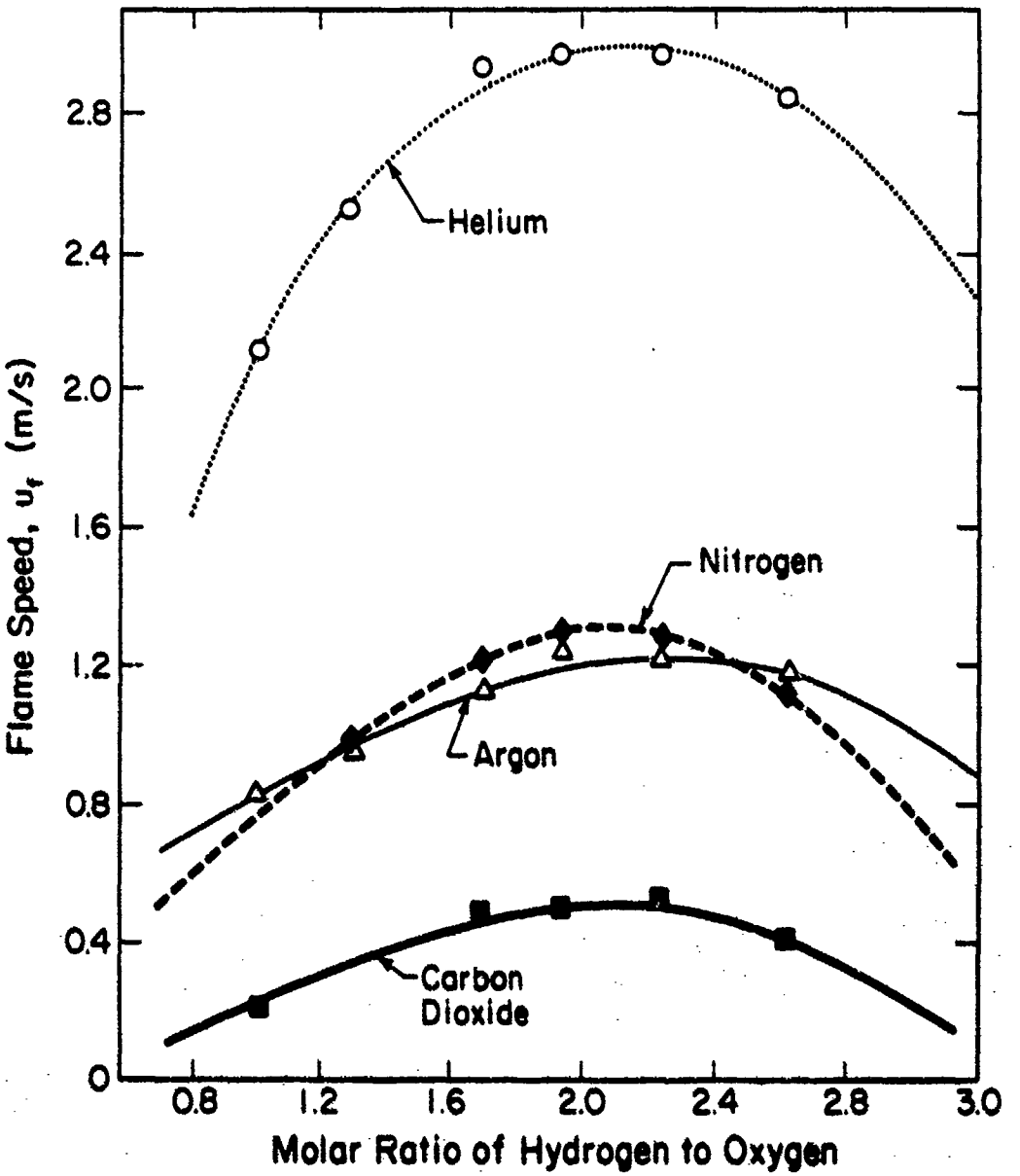

Fig. 28 - Measured flame speeds of hydrogen-oxygen mixtures to which various gases have been added (total amount of third-gas in mixture is 68.24%)

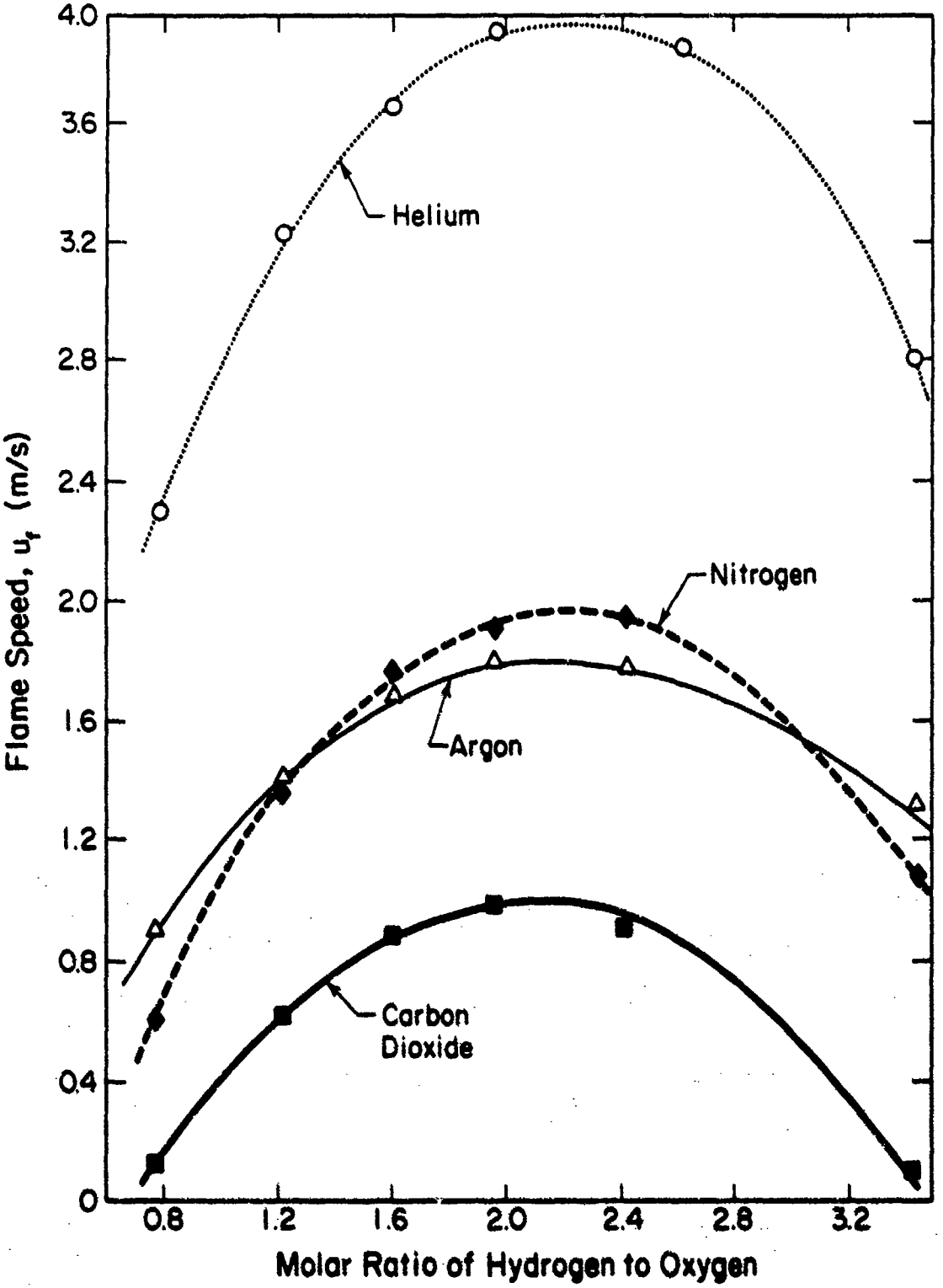

Fig. 29 - Measured flame speeds of hydrogen-oxygen mixtures to which various gases have been added (total amount of third-gas in mixture is 55.64%)

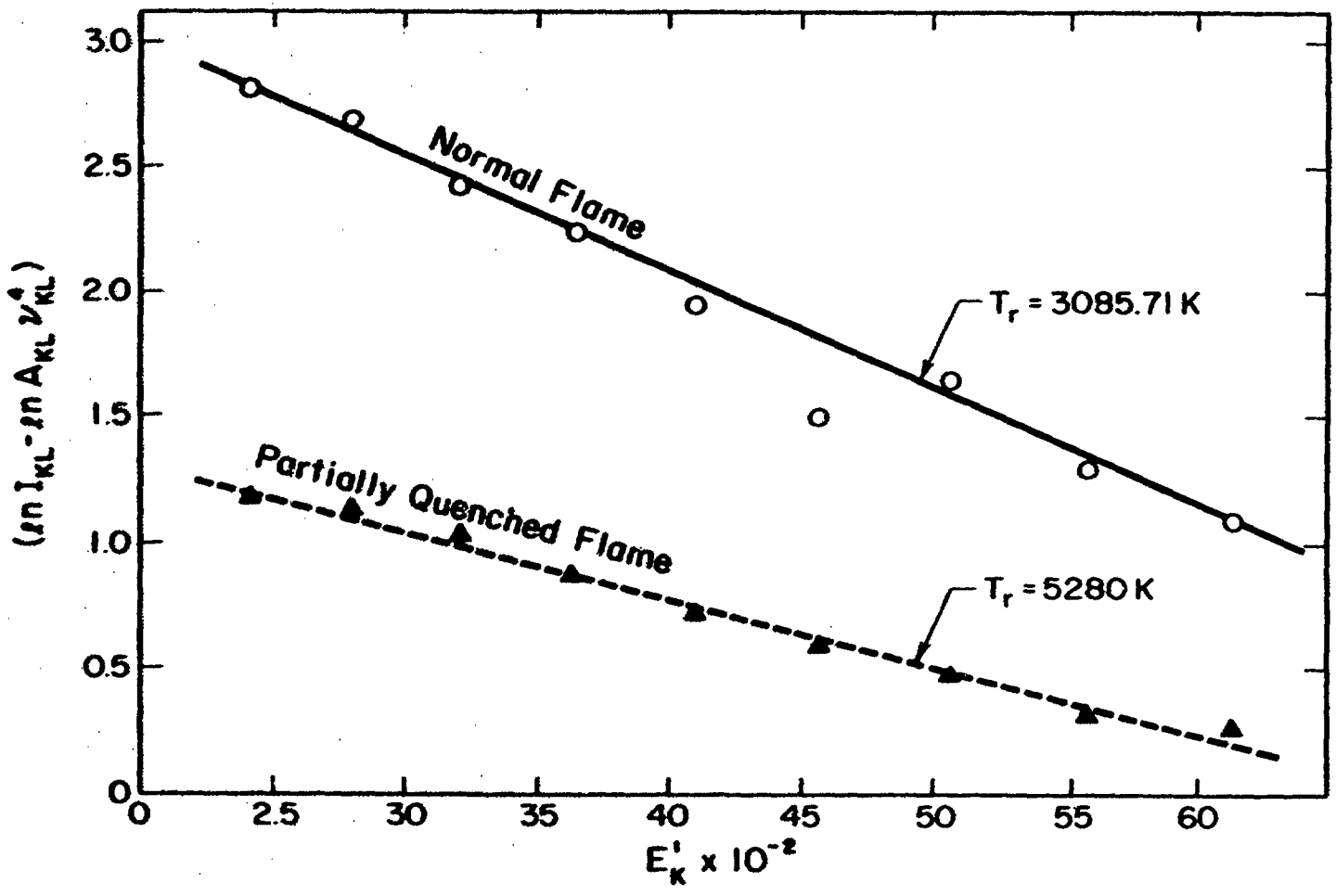

Fig. 30 - Determination of the rotational temperature, T_r, of the flame of a 40% methane and 60% oxygen mixture (based on 4315 Å CH band system)

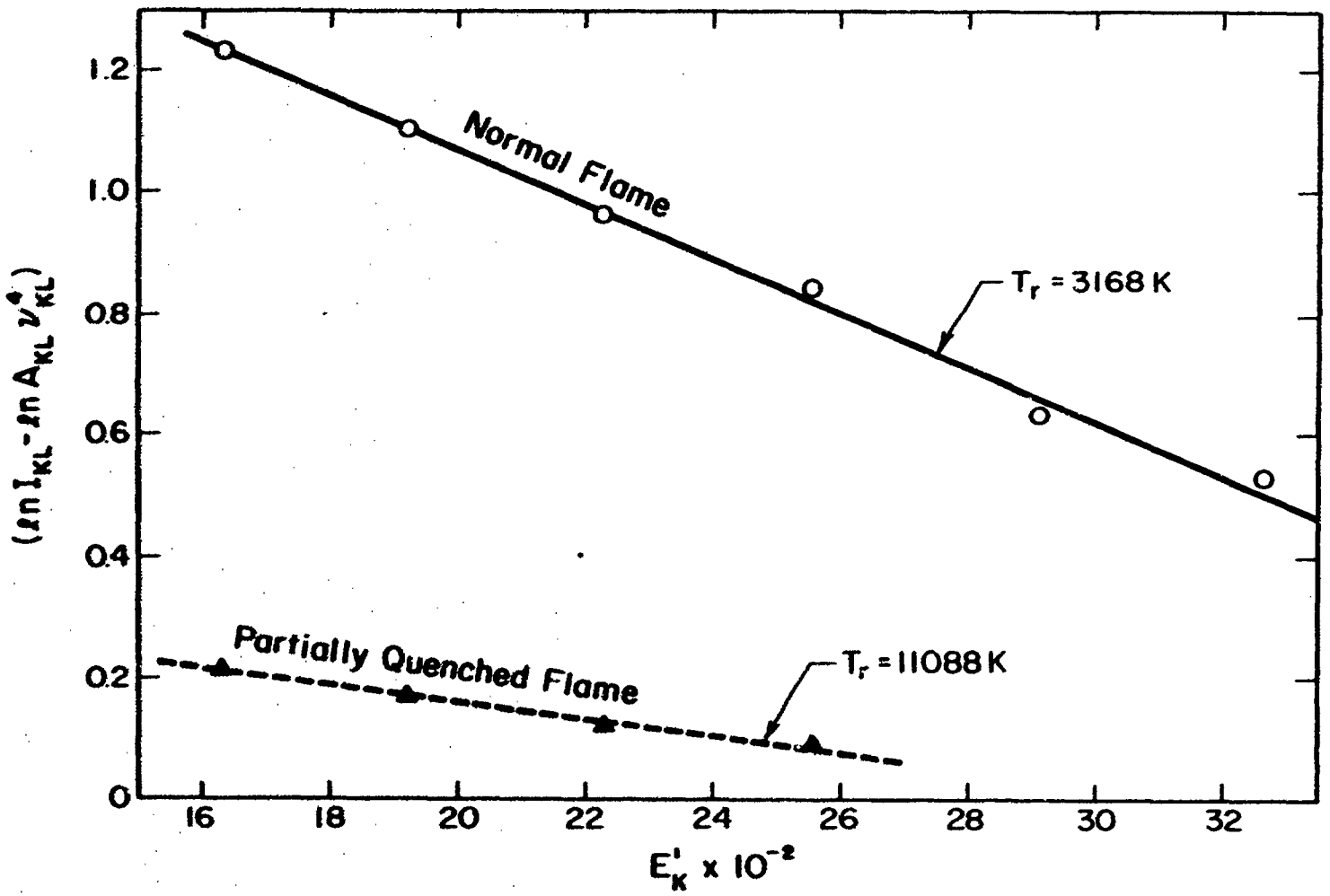

Fig. 31 - Determination of the rotational temperature, T_r, of the flame of a 40% methane and 60% oxygen mixture (based on 3870 Å CH band system)

III. TRANSITION FROM DEFLAGRATION TO DETONATION

Two effects on the transition from deflagration to detonation are being investigated; i.e., (1) the effect of initial gas density, and (2) the effect of turbulence. To assess the contributions of the various properties of the combustible gas mixtures first the flame speeds were measured for the following mixtures: $H_2 + 1/2\ O_2 + X$ where X = He, A, N_2, or CO_2. The measurements were made at an initial temperature of 298 K and an initial pressure of 1 atm. The results are shown in the table below, together with the calculated flame temperatures and C.J. detonation speeds.

X	u_f(m/s)	T_f(K)	$w_1^{C.J.}$(m/s)
He	4.52	2840	3324
A	3.98	2840	2049
CO_2	1.95	2362	1702
N_2	3.40	2708	2092

Then an extensive series of experiments to determine the detonation induction distances of these mixtures at various initial conditions was started. To obtain these distances the pressures behind the flames and their propagation rates were determined at various locations in the detonation tube. Results obtained so far for N_2, He, and A indicate that the induction distances do not seem to vary beyond the accuracy of these measurements. The measured induction distances for these three mixtures range from 1.5 to 2.0 m.

The effect of turbulence on the induction distance was studied in a detonation tube in which the combustible mixture just prior to ignition was agitated by a small fan near the ignitor. The fan was turned off before ignition. The measurements of the induction distances do not indicate a noticeable decrease due to turbulence. However, it appears that the small fan did not agitate the gas sufficiently and most likely set only the gas near the ignitor in motion. Therefore, a different approach will be used for the study of the effect of turbulence; an open-ended tube will be used through which the combustible gases flow as the combustion wave travels (with or against the flow) through the mixture.

REFERENCES

1. Benson, S. W., The Foundations of Chemical Kinetics, McGraw-Hill Book Co., New York (1960).

2. Laidler, K. J., Chemical Kinetics, p. 185, McGraw-Hill Book Co., New York (1950).

3. Gilbert, M., and Altman, D., Sixth Symposium (International) on Combustion, p. 222, Reinhold Publishing Corporation, New York (1957).

4. Taylor, H. S., Combustion Process, p. 132, High Speed Aerodynamics and Jet Propulsion, Vol. II, Princeton, New Jersey (1956).

5. Kanury, M. A., Introduction to Combustion Phenomena, p. 132, Gordon and Breach Science Publishers, New York (1975).